

**Effect of Vanadium Additions on Dispersoid Formation and Performance of
AA6111**

by

Ryan Joseph Miranda

B.S. in Biological Sciences, University of Pittsburgh, 2016

Submitted to the Graduate Faculty of the
Swanson School of Engineering in partial fulfillment
of the requirements for the degree of
Master of Science in Materials Science and Engineering

University of Pittsburgh

2023

UNIVERSITY OF PITTSBURGH

SWANSON SCHOOL OF ENGINEERING

This thesis was presented

by

Ryan Joseph Miranda

It was defended on

March 6, 2023

and approved by

Zachary Harris, Ph. D., Assistant Professor, Department of Mechanical Engineering and
Materials Science

Jung-Kun Lee, Ph. D., Professor, Department of Mechanical Engineering and Materials Science

Thesis Advisor: Wei Xiong, Ph. D., Associate Professor, Department of Mechanical Engineering
and Materials Science

Copyright © by Ryan Joseph Miranda

2023

Effect of Vanadium Additions on Dispersoid Formation and Performance of AA6111

Ryan Joseph Miranda, MS
University of Pittsburgh, 2023

This study presents and investigates the effect of processing variations and alloy additions on the 6xxx series aluminum automotive alloy AA6111. 6xxx series aluminum alloys play an integral role in the automotive industry. Current developments are centered around maintaining high strength while improving bendability and crash performance. AA6111 contains intentional additions of manganese and unintentional additions of chromium which help control the grain structure by forming a population of fine dispersoid particles during high temperature homogenization. These dispersoid particles act as grain boundary pinning particles during recrystallization, which occurs during final solution heat treatment. It is also theorized that these fine dispersoid particles also more evenly distribute strain during deformation, improving formability. Vanadium, like manganese and chromium, will also form dispersoid particles in aluminum. This study aimed to evaluate how modifications to high temperature homogenization time and vanadium additions affect the microstructure and resulting properties of AA6111.

Thermodynamic calculations were used to optimize the homogenization temperature and predict the amount of dispersoid formed during this treatment. Optical Microscopy (OM), Scanning Electron Microscopy (SEM), and Electron Backscatter Diffraction (EBSD) techniques were used to characterize and quantify the dispersoid particles and grain structures.

Optical microscopy was used to evaluate the various samples in the as-homogenized condition. After etching the samples, the etch pits give an initial indication of amount of dispersoids present even though this technique does not have high enough resolution to image the dispersoids themselves.

SEM images were randomly captured on all samples in the as-homogenized condition and used to calculate area fraction of dispersoid present. Vanadium additions led to an increased area fraction of dispersoids when given a 24-hour homogenization treatment. Additionally, scanning electron microscopy energy dispersive spectroscopy (SEM-EDS) identified vanadium in solid solution, in constituent particles, and in dispersoids.

EBSD measured the area-weighted grain size of the samples in the final T6 temper to assess the effect of homogenization time and cold work level on final grain size. In all conditions regardless of cold work, the vanadium additions were able to further reduce the grain size by 2 to 4 microns depending on the condition.

Table of Contents

1.0 Introduction.....	1
2.0 Background	4
3.0 Experimental	9
3.1 Sheet Fabrication.....	10
3.2 Metallographic Examination.....	13
4.0 Results	18
5.0 Discussion.....	42
5.1 Mechanical Properties.....	47
6.0 Conclusions.....	50
7.0 Recommendation and Future Work	52
Bibliography	53

List of Tables

Table 1 Standard AA6111 sales limits and the measured compositions for AA6111 and AA6111 + V.....	9
Table 2 Description of alloy, homogenization time, hot roll gauge, and total cold work percentage.....	12
Table 3 Scheil solidification predictions of the aluminum matrix composition after solidification of the compositions given in Table 1.	18
Table 4 SEM-EBSD area-weighted grain size measurements for AA6111 and AA6111 + V given two homogenization treatments and two levels of cold work, then processed to T6 temper.....	38
Table 5 Tensile test results for the AA6111 and AA6111 + V sheet, given two homogenization treatments and two levels of cold work, then processed to T4 and T6 tempers.....	39

List of Figures

Figure 1 Plot showing formability vs tensile yield strength (TYS) for various aluminum alloy series. Yellow circle represents current AA6111 and purple circle represents AA6111 with increased formability [7].	2
Figure 2 Crystal structure of α-Al₁₂(Mn,Fe,Cr,X)₃Si dispersoid. This dispersoid has a cubic structure, a space group Pm3, 138 atoms in the unit cell, and a lattice parameter a = 12.68 x 10⁻¹⁰m [25].	5
Figure 3 Thermal traces of the homogenization practice used for the AA6111 and AA6111 + V ingots. Ingots were given a 16-hour logarithmic heat up representative of a production scale heat up, 2-hour and 24-hour homogenization, and air-cool.	11
Figure 4 Representative SEM secondary (a,c) and backscattered electron (b,d) images of dispersoid particles present in AA6111 (a,b) and AA6111 + V (c,d) after 24-hour homogenization, captured at 5000X magnification.	14
Figure 5 Representative SEM secondary (a,c) and backscattered electron (b,d) images of dispersoid particles present in AA6111 (a,b) and AA6111 + V (c,d) after 24-hour homogenization, captured at 10000X magnification.	15
Figure 6 Thermo-Calc equilibrium phase fraction predictions for homogenization of AA6111 at 560°C (1040°F), based on the matrix composition of AA6111 given in Table 2....	19
Figure 7 Crystal structure of α-Al₁₈Mg₃V₂ dispersoid. This dispersoid has a cubic structure, a space group Fd3m, 184 atoms in the unit cell, and a lattice parameter a = 14.60Å [13].	20

Figure 8 Thermo-Calc equilibrium phase fraction predictions for homogenization of AA6111 + V at 560°C (1040°F), based on the matrix composition of AA6111 + V given in Table 2..... 21

Figure 9 SEM-EDS image suggesting the presence of α -Al₁₂(Fe,Mn,X)₃Si constituent in AA6111..... 22

Figure 10 SEM-EDS image suggesting the presence of α -Al₁₂(Fe,Mn,X)₃Si constituent in AA6111 + V..... 23

Figure 11 X-ray diffraction obtained from samples of AA6111 and AA6111 + V showing the various peaks. The large peaks at roughly 38.5° and 45° are the aluminum peaks and are present in both samples. The peaks present in both samples at roughly 19°, 20°, 22°, 25.5°, 27.5°, 31.5°, 36.5°, 42°, and 43° are the α -Al₁₂(Fe,Mn,X)₃Si peaks representing the constituent and dispersoid. The peaks at 41° and 43.5° in AA6111 + V, but not in AA6111 match two of the major E-phase peaks, however the minor E-phase peaks are not identifiable and the presence of E-phase cannot be confirmed with XRD. 24

Figure 12 SEM map showing the presence of vanadium in grain interiors. 25

Figure 13 SEM-EDS showing the presence of V-bearing constituent on grain boundary... 26

Figure 14 SEM map showing presence of V-bearing dispersoid particle..... 27

Figure 15 Optical metallography of (a, b) AA6111 and (c, d) AA6111 + V samples given (a, c) 2h and (b, d) 24 h homogenization practices, revealing etch pits associated with heterogenous dispersoid population..... 29

Figure 16 Representative SEM-BSE image from AA6111 with a 24-hour homogenization used for dispersoid quantification using ImageJ software..... 30

Figure 17 Average dispersoid effective particle diameter for the AA6111 and AA6111 + V given a 2-hour and 24-hour homogenization. Comparison shows a statistically significant difference in effective particle diameter within each alloy for the two different homogenization practices. Error bars reflect one standard deviation..... 31

Figure 18 Comparison of total dispersoid percent area in AA6111 and AA6111 + V homogenized for 2-hours and 24-hours. Comparison shows a statistically significant increase in dispersoid percent area between AA6111 homogenized for 2-hours and 24-hours. Error bars reflect one standard deviation..... 32

Figure 19 Histogram showing the amounts of particles measured in AA6111 when homogenized for 2-hours and 24-hours. Comparison shows both homogenizations yield similar particle size populations in differing amounts. Error bars reflect one standard deviation. 33

Figure 20 Histogram showing the amounts of particles measured in AA6111 + V when homogenized for 2-hours and 24-hours. Comparison shows both homogenizations yield similar particle size populations in differing amounts. Error bars reflect one standard deviation. 34

Figure 21 EBSD images of (a, c) AA6111 and (b, d) AA6111 + V samples all given 43% cold work reduction and (a, b) given 2-hour homogenization and (c, d) given 24-hour homogenization showing slight grain refinement with the addition of vanadium.... 36

Figure 22 EBSD images of (a, c) AA6111 and (b, d) AA6111 + V samples all given 68% cold work reduction and (a, b) given 2-hour homogenization and (c, d) given 24-hour homogenization showing slight grain refinement with the addition of vanadium.... 37

Figure 23 Comparison of the n-value (4-6%) of AA6111 and AA6111 + V given a 2-hour homogenization, 43% and 68% cold work reductions, and aged to the T4 condition. Values show no significant benefit to n-value by adding vanadium to AA6111. Error bars reflect one standard deviation. 40

Figure 24 Comparison of the n-value (4-6%) of AA6111 and AA6111 + V given a 24-hour homogenization, 43% and 68% cold work reductions, and aged to the T6 condition. Values show no significant benefit to n-value by adding vanadium to AA6111. Error bars reflect one standard deviation. 41

Figure 25 Area weighted grain size versus f/r parameter for both compositions, homogenization times, and cold work levels. The f/r parameter provides a representation of Zener drag in the material. The baseline AA6111 material does not follow the expected result that an increase in f/r value should increase the Zener drag effect and decrease grain size. AA6111 + V does follow the expected trend. 46

Figure 26 Yield strength variation in a 6xxx series aluminum alloy in the T4 temper compiled by Burger et al., 1995. The slope of the trendline was found to not be statistically significant from zero, indicating no strength increase due to grain size reduction from 46 to 27 μ m [6]. 49

1.0 Introduction

Currently, the majority of automotive aluminum sheet that is generated is either AA5xxx or AA6xxx, trending towards increased volumes of AA6xxx due to its higher versatility [7]. 6xxx series aluminum alloys are characterized by their major alloying elements, magnesium, and silicon. These alloys are known for being heat treatable, having good strength values, moderate formability, dent resistance, corrosion resistance, and weldability [1]. This alloy series' ability to have high formability in the T4-type tempers and good strength and dent resistance in the aged tempers is the reason why it is so widely used in different automotive applications. According to the American National Standard Alloy and Temper Designation Systems for aluminum, H351./H35.1(M), The Aluminum Association, 2017 edition, (May 12, 2017), the T4 temper is the condition following a solution heat treatment plus natural aging [2]. Additionally, the use of aluminum allows for light weighting vehicles which increases the fuel efficiency. Figure 1 shows formability vs strength for 5xxx, 6xxx, and 7xxx series aluminum alloys [7]. As shown by this figure, 6xxx series aluminum alloys typically fall in the high strength range while still maintaining moderate formability.

Today, the 6xxx series aluminum alloys used most in the automotive industry are AA6016, AA6111, AA6022, and AA6061, however, the main limitation of these current high strength 6xxx series alloys are their limited, moderate formability [1]. According to the literature, typical property values for AA6111 are: TYS ~150 MPa (T4), elongation 26% (T4) TYS ~340 MPa (T6), and elongation 12% (T6) [9]. AA6111 is represented by the yellow circle superimposed on Figure 1.

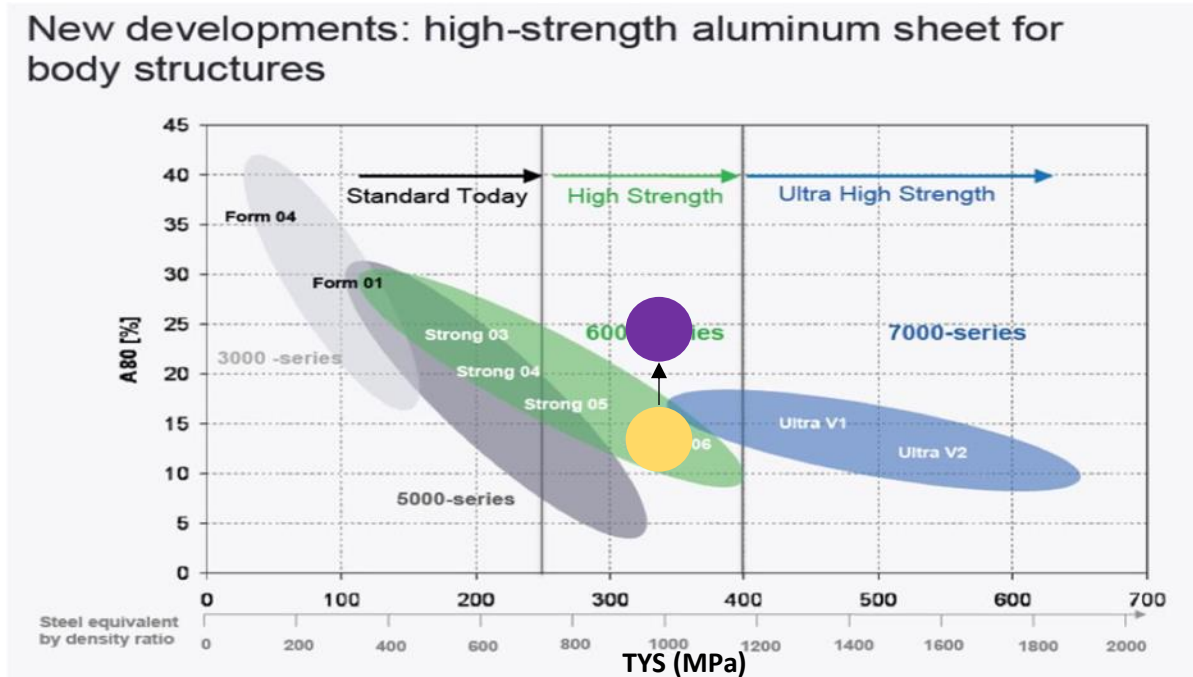


Figure 1 Plot showing formability vs tensile yield strength (TYS) for various aluminum alloy series. Yellow circle represents current AA6111 and purple circle represents AA6111 with increased formability [7].

One of the key microstructural features of aluminum automotive alloys is grain structure as it can affect many different aspects of the materials performance. Depending on the application, AA6111 can be riveted in the T6-temper, which is why controlling grain structure is important when trying to manipulate formability. One way to control the grain structure is by manipulating the size and distribution of the dispersoid particles formed during homogenization. Dispersoids are high temperature precipitates that form during purposefully designed homogenization treatments [9]. Dispersoids act as grain pinning particles during solution heat treatment that inhibit the development and growth of new grains during recrystallization.

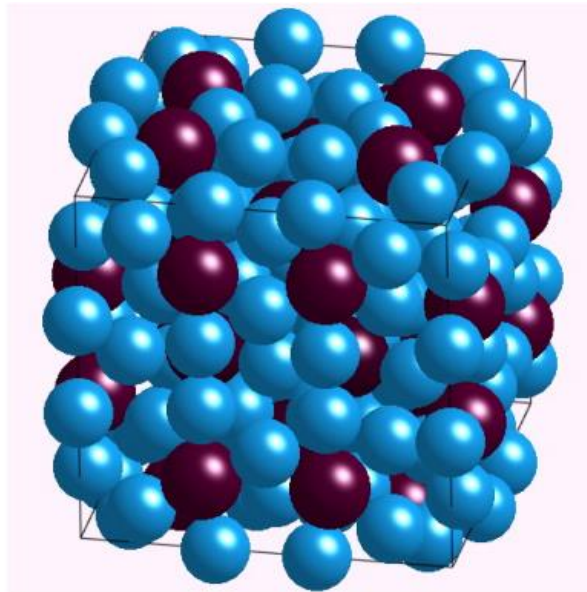
There is limited precedence in the literature discussing the use of vanadium in 6xxx series aluminum as a dispersoid forming element. In aluminum, vanadium participates in a peritectic

reaction with aluminum, and hence tends to be enriched in grain interiors. Vanadium, like manganese and chromium, can also both be present in constituent particles and act as a dispersoid forming element when added to aluminum. Available literature discusses the presence and effect of vanadium in the large constituent particles but fails to discuss the role of vanadium in the much smaller, more prevalent dispersoid particles. If the vanadium is present in these dispersoid particles and leads to an increased number of these particles in the microstructure, it could be beneficial by decreasing grain size and improving forming properties by more evenly distributing strain during deformation. An in-depth study of these particles and their effect on microstructure and mechanical properties is necessary to more fully understand the role of vanadium in 6xxx series aluminum alloys.

The purpose of this study is to produce and examine AA6111 with and without vanadium additions. This study will evaluate the impact on size, distribution, and amount of dispersoids formed in different homogenized conditions and measure the various grain structures these produce with differing amounts of cold work. Tensile properties, including n-value, TYS, UTS, and elongation will be used to evaluate impact on strength and formability.

2.0 Background

AA6111 is a high strength 6xxx series aluminum alloy. The main alloying elements in 6xxx series aluminum are magnesium and silicon. Magnesium and silicon are present and form the main strengthening phases during aging. According to the literature, the precipitation sequence in 6xxx series aluminum alloys begins when silicon and magnesium clusters form from the solid solution in what are known as GP zones. These GP zones then form needlelike β' (Mg_2Si) which at higher temperatures will undergo diffusion-less phase transformation to the rod-shaped β (Mg_2Si) [9]. The β' Mg_2Si phase is the main strengthening phase in 6xxx series aluminum has the greatest impact on the material's TYS and UTS. Furthermore, the literature shows that copper additions also play a role in 6xxx series aluminum alloys' strengthening behavior. During aging, formation of the copper based, lathlike Q' phase forms during peak aging, suggesting there is copper remaining in solid solution that can increase the strength via solid solution hardening. Additionally, copper creates a finer precipitate structure which leads to increased strength after artificial aging [21]. Other alloying elements are also added in various smaller amounts. The main phase formed when manganese and chromium additions are present is the $\alpha\text{-Al}_{12}(\text{Mn,Fe,Cr})_3\text{Si}$ which can appear as both constituent and dispersoid phases. The $\alpha\text{-Al}_{12}(\text{Mn,Fe,Cr})_3\text{Si}$ phase has a cubic structure, a space group of Pm3, 138 atoms in the unit cell, and a lattice parameter of $a = 12.68 \times 10^{-10}\text{m}$ (Figure 2) [22].



Compound	a
α -Al-Mn-Si	1.268

Figure 2 Crystal structure of α -Al₁₂(Mn,Fe,Cr,X)₃Si dispersoid. This dispersoid has a cubic structure, a space group Pm3, 138 atoms in the unit cell, and a lattice parameter $a = 12.68 \times 10^{-10}$ m [25].

Iron is present as a normal impurity in aluminum. The presence of iron has deleterious effect on mechanical properties and corrosion, but it would be economically prohibitive to eliminate it all together.

The processing of aluminum plays a critical role in the resulting microstructure. The cast structure of aluminum contains both soluble and insoluble constituent in the interdendritic regions. During homogenization of the ingot, soluble constituents dissolve and dispersoids form. Dispersoids tend to be somewhat non-uniform because of solute partitioning during solidification. The purpose of the dispersoids is to control grain structure, not necessarily to provide strength. The ingot then goes through a combination of hot rolling and cold rolling. An intermediate anneal

between hot rolling and cold rolling can be used depending on the desired final grain size and texture. A solution heat treatment is used to dissolve soluble phases which have precipitated during hot rolling to utilize all the Mg and Si possible for strengthening. Recrystallization also takes place during the solution heat treatment. The size and amount of dispersoids present will affect the final grain size through Zener drag or Zener pinning [19]. This concept suggests that the higher the amount of evenly dispersed second phase particles and the finer their size, the smaller the expected grain size. This final grain structure has a direct impact on the performance of the material [11].

There is limited precedence in the literature describing the impact of vanadium in 6xxx series aluminum alloys. The purpose of this research was to add vanadium to AA6111 and document the effects. For example, Meng et al., 2013, researched the effect of vanadium on the microstructures and mechanical properties of Al-Mg-Si-Cu-Cr-Ti alloy. In this work Meng et al., 2013 created two Al-4 weight percent vanadium master alloys by adding Al-50V to high purity (99.99 weight percent) aluminum. Master alloy A was prepared with fast cooling while master alloy B was prepared with slow cooling. The main V-containing phase in master alloy A was Al_3V , while the main V-containing phase in master alloy B was $Al_{10}V$. Three experimental alloys were then created. The first was the baseline alloy (Al-1.6Mg-1.2Si-1.1Cu-0.16Cr-0.03Ti) which contained no vanadium additions. The second experimental alloy was the baseline alloy combined with master alloy A to achieve a baseline composition with 0.15 weight percent vanadium additions. The third experimental alloy was the same as the second but used master alloy B to achieve the desired vanadium content. The ingots were then homogenized at 540°C for 24-hours before being extruded and aged to the T6 temper. In the as-cast condition, vanadium was identified using EDS in the constituent phase located on the grain boundaries. $Al(V,Cr,Ti)Si$ dispersoids were identified using TEM in the baseline alloy with vanadium additions from master alloy A, but

not in the baseline alloy with vanadium additions from master alloy B. Meng et al., 2013 discusses that the dispersoids present in the alloy with vanadium additions from master alloy A will make the distribution of dislocations more homogenous and reduce the number of nucleation sites for recrystallization. The small sizes and high number densities create small inter-particle spacing, which will pin the subgrains and inhibit recrystallization [20]. The conclusion of this work is that vanadium additions using master alloy A result in increased strength by extrusion effects, solution strengthening, and dispersion strengthening. While this work was able to identify Al(V,Cr,Ti)Si dispersoids, there was no work to identify the impact of those particles on grain structure in a final product.

Lech-Grega et al., 2015, evaluated the mechanical properties of Al-Mg-Si-Cu aluminum alloys with 0.1 and 0.2 weight percent additions of vanadium. The ingots in this work were not homogenized before extrusion and were solution heat treated and artificially aged to multiple tempers. TEM identified V containing precipitates (Al-Si-Fe-Cu-Cr-V, Al-Mg-V, and Al-Cu-Fe-Si-V) ranging in size from 50nm to 500nm, but these are not quantified and their influence on mechanical properties is not discussed. Conclusions of this work state that vanadium additions slightly reduce the mechanical properties (TYS, UTS, and elongation) of the alloy [15]. In this work the presence and role of dispersoid particles is not mentioned. In this study, there was no homogenization treatment, thus the relatively short time spent at elevated temperature in preparation for extrusion appears to have been sufficient to bring out the vanadium-bearing dispersoids. The fine vanadium-containing particles again were not quantified nor their role in inhibiting recrystallization or potential contributions to increased strength discussed.

Lastly, Lech-Grega et al., 2012, studied vanadium additions of 0.2 and 0.4wt.% to a 6xxx series aluminum alloy. Ingots were homogenized for 8, 24, and 100 hours at 570°C. They observed

large angular $\text{Al}_{18}\text{Mg}_3\text{V}_2$ precipitates that formed during solidification. They reported that homogenization had no effect on the morphology of these large (50 μm) vanadium bearing constituent particles. Lech-Grega, 2012 reported that prior to homogenization, the vanadium free alloy had slightly higher yield strength, but after homogenization the vanadium-bearing alloy had the higher yield strength [16]. While this paper is studying the effect of homogenization when vanadium is added to a 6xxx series aluminum alloy, the formation of dispersoid particles during homogenization is not evaluated.

Although there are numerous authors in the literature that have studied the effects of vanadium additions to 6xxx series aluminum, there is limited understanding of the impact of vanadium additions on the type, size, and amount of additional dispersoids produced and their impact on grain structure and properties in the final product, hence this study will address those questions. This study will evaluate the as-cast, 2-hour homogenized, 24-hour homogenized, and T6 microstructures of AA6111 and AA6111 + 0.1wt.% vanadium. In the homogenized condition, this study will quantify and compare the size distribution and area fraction of dispersoids present in all homogenization conditions for both alloys. The grain structure will be measured in the T6 condition to evaluate the grain pinning effectiveness of the dispersoids that are formed. TYS, UTS, elongation, and n-value will also be compared in the T6 temper for both alloys and all homogenization conditions to evaluate any differences in mechanical properties. This study will fill the gaps in the current literature that currently exist when studying vanadium additions to 6xxx series aluminum alloys.

3.0 Experimental

Thermo-Calc was used as a preliminary prediction tool to give initial insight on which phases would form and in what amounts in each alloy of interest. First, a Scheil solidification calculation was run on the compositions given in Table 1 to determine how much solute would remain in the matrix after solidification and hence would be available to form dispersoids during homogenization.

Table 1 Standard AA6111 sales limits and the measured compositions for AA6111 and AA6111 + V.

Alloy Composition (wt%)							
Alloy	Si	Fe	Cu	Mn	Mg	Cr	V
AA6111 limits	0.6-1.1	0.40 max	0.50-0.90	0.10-0.45	0.50-1.0	0.10 max	0.15 max
AA6111	0.96	0.27	0.70	0.21	0.80	0.08	-
AA6111+V	0.96	0.27	0.67	0.21	0.82	0.09	0.11

Both compositions are within the sale limits of AA6111. Chromium and iron additions were intentionally added in the laboratory casting as these elements would be expected due to scrap reuse in industry. After this, an equilibrium calculation was run on the matrix composition after Scheil solidification to determine which phase or phases are present and in what amounts.

3.1 Sheet Fabrication

For this investigation, 12" long x 3.5" wide x 2.5" high ingots were cast and their compositions are listed in Table 1. These compositions were obtained by quantometer analysis. Two ingots were cast of each composition. The ingots were then scalped.

After machining, a hole was drilled ¼" deep into two ingots, into which thermocouples were placed and secured. The ingots were then loaded into a furnace for homogenization treatment. For this experiment, two homogenization times were chosen to represent the shortest reasonable industrial homogenization practice, two hours, and a long industrial homogenization practice, 24 hours. From room temperature, the furnace was programmed to follow a 16-hour logarithmic heat up schedule, representative of the heat-up rate expected in an industrial size ingot, to a homogenization temperature of 560°C (1040°F). Once this temperature was reached, one ingot of each composition was homogenized at 560°C (1040°F) for two hours before they were removed from the furnace and allowed to air cool. The remaining two ingots were left in the furnace and homogenized at 560°C (1040°F) for a total of 24 hours before they were also removed from the furnace and allowed to air cool. Concurrently, small ingot slices received the same homogenization practice as the full ingots - but received a cold-water quench when removed from the furnace to freeze the high temperature microstructure for evaluation using optical metallography and scanning electron microscopy. This was done to avoid the precipitation of coarse Al-Mg-Si-Cu particles which would occur in slow, air cooling of the ingots and would make it difficult to image the dispersoids that formed during homogenization. A thermal trace for the ingot homogenization temperature versus time can be seen in Figure 3.

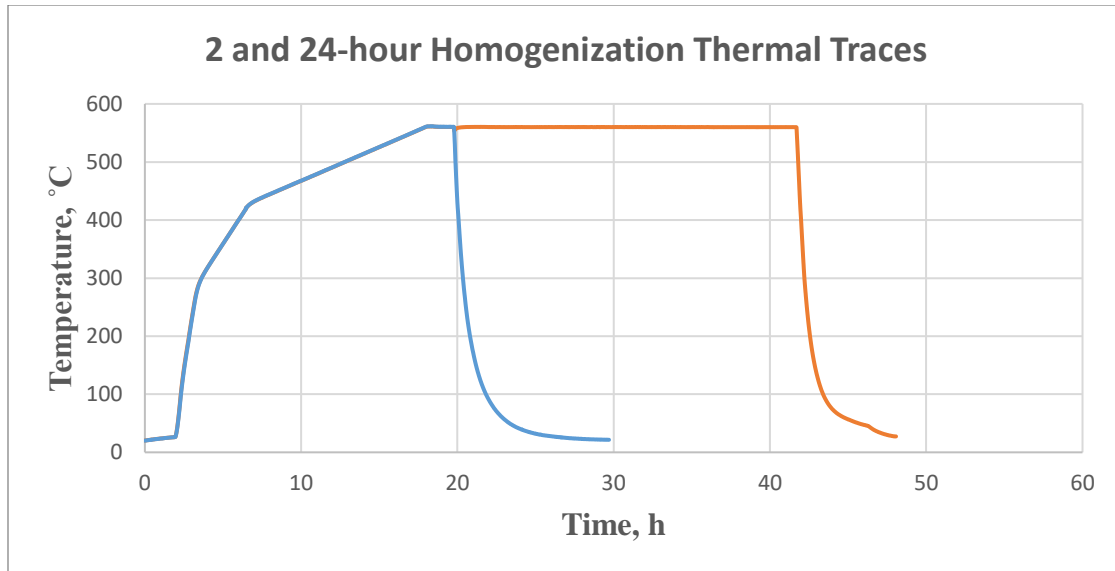


Figure 3 Thermal traces of the homogenization practice used for the AA6111 and AA6111 + V ingots. Ingots were given a 16-hour logarithmic heat up representative of a production scale heat up, 2-hour and 24-hour homogenization, and air-cool.

In industry, an ingot would typically be taken directly from the homogenization furnace to be hot rolled. To mimic this, the homogenized ingots were reheated to 560°C and allowed to stabilize for one hour before hot rolling. Each ingot was then removed from the reheat furnace one at a time and placed on the rolling mill. Each piece was rolled from 63.5mm (2.5”) down to 6.35mm (0.250”) using eight passes. Each 6.35mm thick piece was cooled and cut in half. One half was then reheated to 560°C and further hot rolled from 6.35 to 3.56mm (0.140”). This was repeated for all four ingots resulting in eight total pieces. All eight pieces were subsequently cold rolled to a final thickness of 2.03mm (0.080”), providing two cold work percentages for each condition: 43% and 68% (Table 2).

Table 2 Description of alloy, homogenization time, hot roll gauge, and total cold work percentage.

Sample ID	Alloy	Homogenization Time	Hot roll gauge (in.)	Cold Work Percentage
7072810	AA6111	2 hours	0.240"	68%
7072811	AA6111	2 hours	0.140"	43%
7072812	AA6111	24 hours	0.240"	68%
7072813	AA6111	24 hours	0.140"	43%
7072814	AA6111 + V	2 hours	0.240"	68%
7072815	AA6111 + V	2 hours	0.140"	43%
7072816	AA6111 + V	24 hours	0.240"	68%
7072817	AA6111 + V	24 hours	0.140"	43%

The metal was then cut into 304.8mm (12") long x 101.6mm (4") wide sections for solution heat treatment. The furnace was set to 560°C and once it reached temperature, sections were placed into the furnace and solution heat treated for eight minutes. After eight minutes, the sections were removed from the furnace and cold water quenched. This process was repeated for all the sections. Specimens were then sheared from these sections and allowed to naturally age for 7 days prior to tensile testing. According to the American National Standard Alloy and Temper Designation Systems for aluminum, H351./H35.1(M), The Aluminum Association, 2017 edition, (May 12, 2017), this condition is referred to as the T4 temper [2].

The remaining sections were then precipitation strengthened by placing them in a hot furnace set to 180°C for eight hours. According to the American National Standard Alloy and Temper Designation Systems for Aluminum, H351./H35.1(M), The Aluminum Association, 2017 edition, (May 12, 2017), this condition is referred to as the T6 temper [2]. Specimens were also sheared in this temper for SEM electron back scatter diffraction analysis and tensile testing.

3.2 Metallographic Examination

The ingot slices that were homogenized and cold water quenched were prepared for optical metallography and SEM evaluation. The samples were mounted and polished following standard aluminum polishing procedures. Prior to optical metallography evaluation, the mounts were etched in 0.5% HF for 25 seconds. Representative images were taken at various magnifications to show the effects of the different homogenization times. Additional as-polished samples were examined in the SEM. Images for particle analysis were collected by setting up an 81-image grid on the specimen. Each image had a 300% overlap at 2000X magnification to ensure particles would not be captured in multiple images. Twenty-four random images were captured from the larger 81-image grid. Additionally, energy dispersive x-ray spectroscopy (EDS) was conducted on the samples to identify the constituent phases present on the grain boundaries. Representative dispersoid images were also captured at 5000X and 10000X to get a better understanding of size and morphology of these particles (Figure 4 and Figure 5).

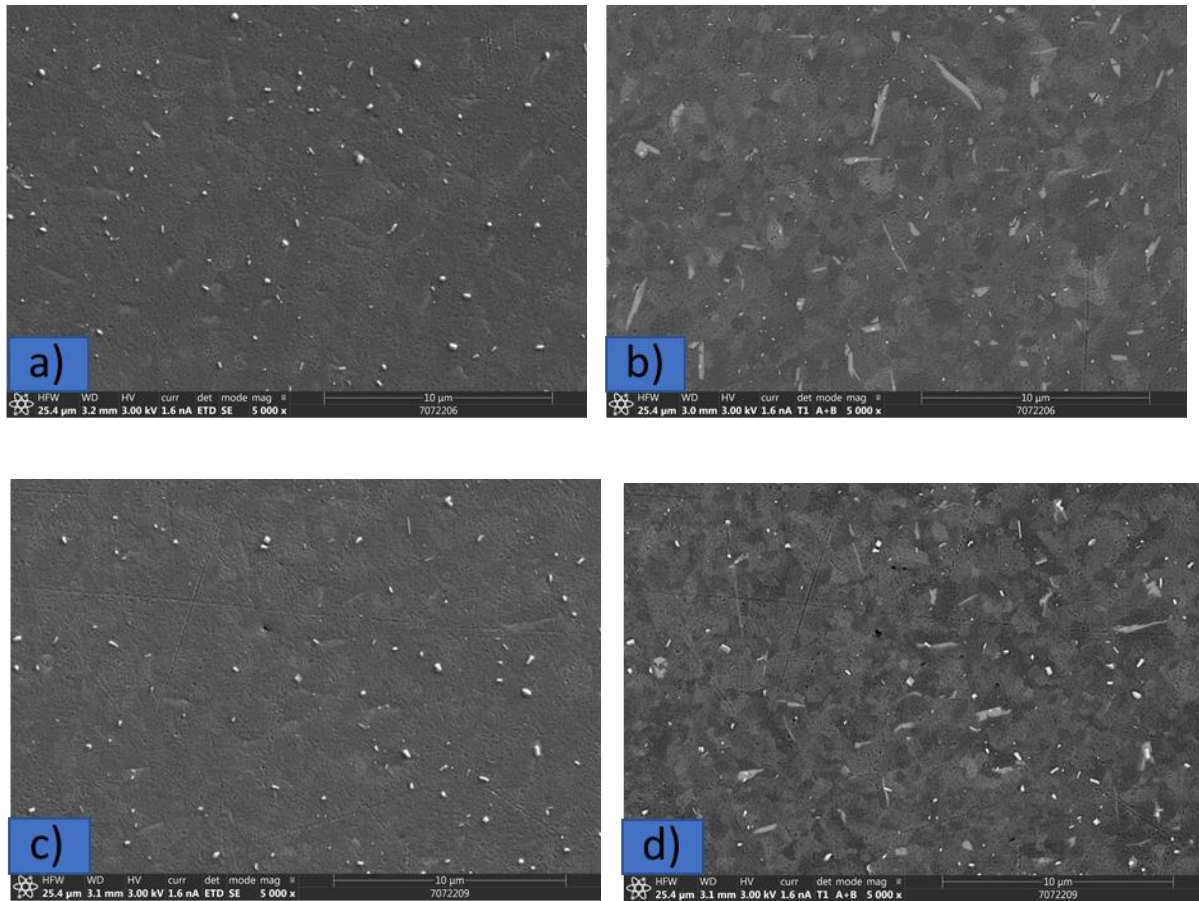


Figure 4 Representative SEM secondary (a,c) and backscattered electron (b,d) images of dispersoid particles present in AA6111 (a,b) and AA6111 + V (c,d) after 24-hour homogenization, captured at 5000X magnification.

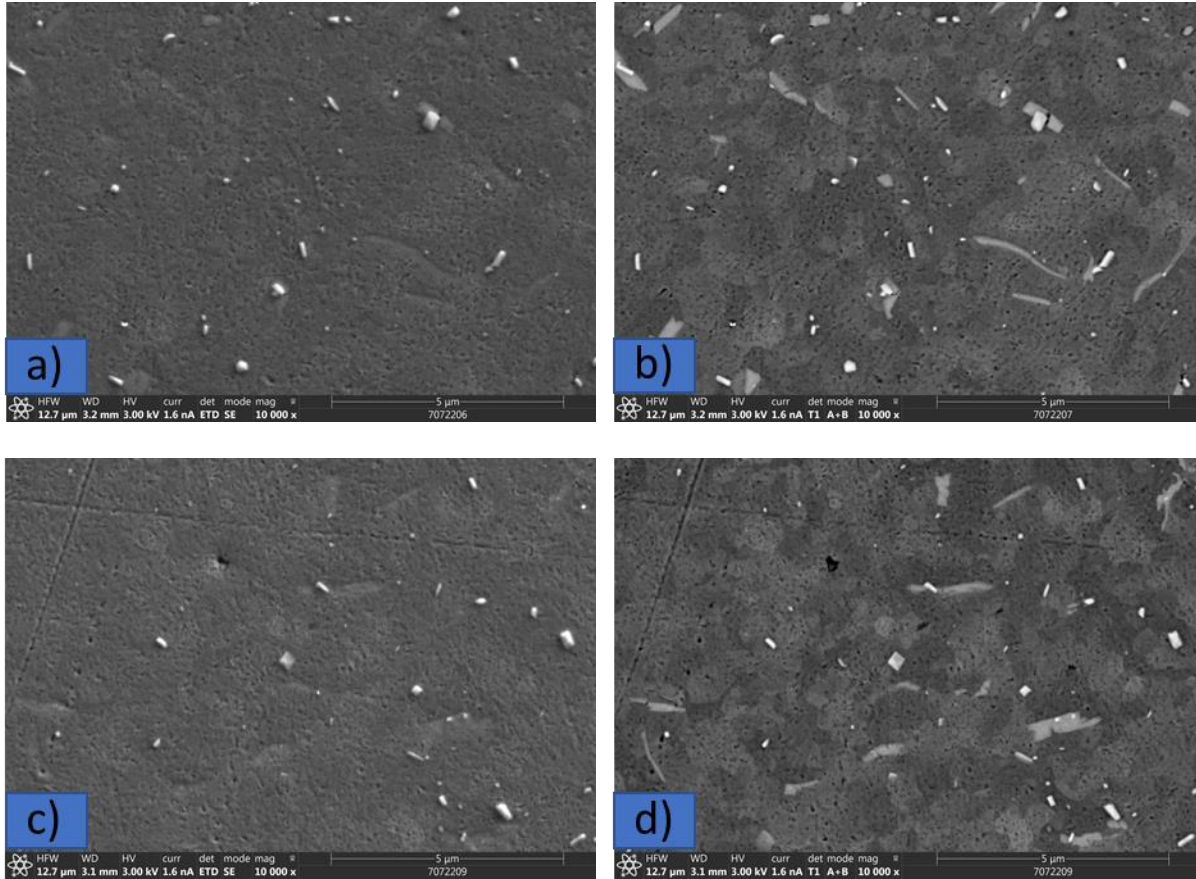


Figure 5 Representative SEM secondary (a,c) and backscattered electron (b,d) images of dispersoid particles present in AA6111 (a,b) and AA6111 + V (c,d) after 24-hour homogenization, captured at 10000X magnification.

Additionally, the as-polished samples were used to identify vanadium in solid solution, in constituent particles, and in dispersoid particle which will be discussed in further detail later.

The image sets collected during SEM analysis were used for dispersoid particle analysis in the various homogenized conditions. Five to ten images per condition were analyzed, purposefully avoiding images of grain boundary areas that are void of dispersoid particles due to the large constituent particles on the grain boundaries removing solute from the aluminum matrix. The five to ten selected images were processed and analyzed within ImageJ. The pixel size used for this

analysis was 21nm so each pixel represents an area of 441nm². A minimum of five-pixel units, or 2205 nm², was set for a particle to be identified. This analysis produced data to calculate area percent of the dispersoids, effective dispersoid diameters, and dispersoid size distributions, where the effective dispersoid diameter is the diameter of a circle having the same area as an individual dispersoid. This process was repeated on every image and the data was then averaged for all the five to ten images.

Specimens collected in the T6 condition were prepared for electron backscattered diffraction (EBSD) analysis. This analysis gave insight on grain size and shape of the different conditions of the material. EBSD measures grain size and shape by using a critical misorientation angle. If the misorientation angle is higher than the critical misorientation angle, the software recognizes this as a grain boundary. The software then analyzes the pixels and their misorientation angles to create grains. With this information, the software can then calculate grain size and its shape can be determined by analysis of the map. In this work, the area weighted measure of grain size was utilized. “Area weighted average grain size” is calculated by the following equation:

$$d\text{-bar} = (\sum_{i=1}^n A_i d_i) / (\sum_{i=1}^n d_i) \quad (3-1)$$

Here, A_i is the area of each individual grain and d_i is the calculated individual grain size assuming the grain is a circle and $d\text{-bar}$ is the area-weighted average grain size. In conjunction with EBSD, x-ray diffraction (XRD) Guinier analysis was conducted on both compositions in the 24-hour homogenized condition to confirm the phases predicted by Thermo-Calc are the phases present in the material. Guinier analysis is an XRD method where the result is an XRD scan that is interpreted by analyzing diffraction peaks, like conventional XRD. Guinier analysis uses a

strip of film as the detector and collects all the x-rays at once. The x-rays appear as lines on the film which are digitized and the diffraction peaks are analyzed. Guinier analysis was chosen for this experiment over traditional 2-theta analysis because of its higher phase sensitivity, or ability to identify components with low concentrations more easily.

Tensile testing was conducted per ASTM E8/E8M-16a and B557-15 in the longitudinal direction for both the T4 and T6 tempers for all four conditions of both compositions. Specimens were standard dog-bone type, 225.4mm (8.875”) long by 22.2mm (0.875”) wide with a 12.7mm (0.5”) wide gauge section.

4.0 Results

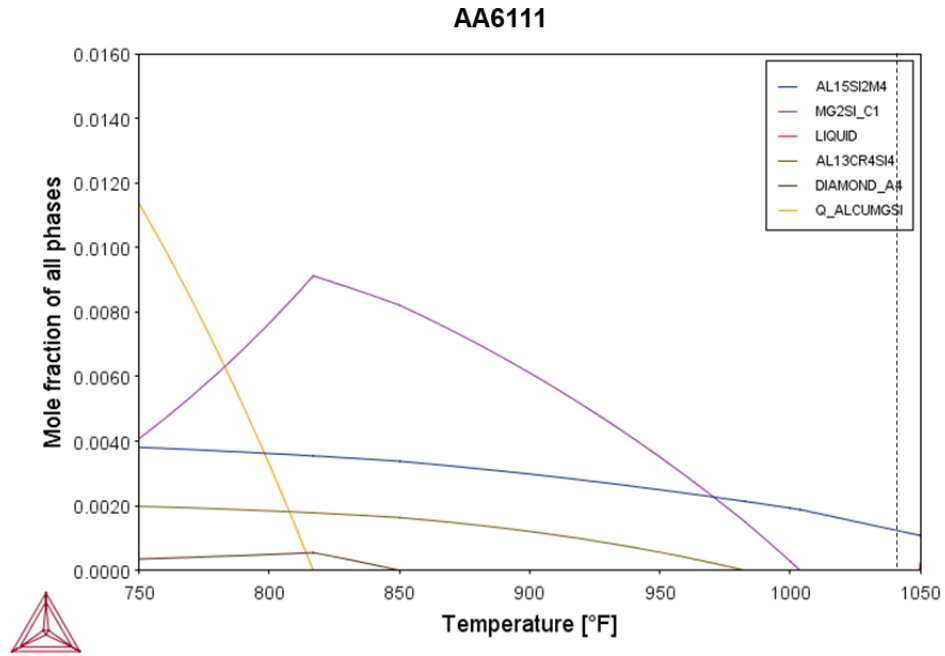
The Scheil calculation run within Thermo-Calc predicts which phases and their volume percentages would form during solidification, more importantly showing the amount of dispersoid-forming elements (Mn, Cr, and V) remaining in solution. The amount of dispersoid forming elements available in the aluminum matrix composition after solidification in AA6111 is 0.141 weight percent Mn and 0.080 weight percent Cr. Similarly, the amount of dispersoid forming elements available in the aluminum matrix composition after solidification in AA6111 + V is 0.140 weight percent Mn, 0.079 weight percent Cr, and 0.098 weight percent V (Table 3).

Table 3 Scheil solidification predictions of the aluminum matrix composition after solidification of the compositions given in Table 1.

Aluminum Matrix Composition After Solidification (wt%)							
Alloy	Si	Fe	Cu	Mn	Mg	Cr	V
AA6111	0.255	0.010	0.253	0.141	0.425	0.080	
AA6111+V	0.236	0.010	0.207	0.140	0.421	0.079	0.098

The Scheil calculation indicates that in both compositions roughly 0.07 weight percent Mn will be used to form either $\text{Al}_6(\text{Fe},\text{Mn})$ or $\alpha\text{-Al}_{12}(\text{Fe},\text{Mn})_3\text{Si}$ constituent. Equilibrium calculations predict 0.13 mole percent, or roughly 0.11 volume percent, $\alpha\text{-Al}_{12}(\text{Fe},\text{Mn},\text{X})_3\text{Si}$ dispersoid phase formation during homogenization in AA6111 (Figure 6) and 0.11 mole percent $\alpha\text{-Al}_{12}(\text{Fe},\text{Mn},\text{X})_3\text{Si}$ dispersoid phase formation during homogenization in AA6111 + V, where X is Cr and possibly other transition elements, like V, which may be present and could substitute for

Fe or Mn in the α -Al₁₂(Fe,Mn,X)₃Si phase.



Equilibrium Phase Fraction at 560°C (1040°F) (mol %)				
Alloy	Al ₁₃ Cr ₄ Si ₄	Al ₁₅ Si ₂ M ₄	CrSi ₂ _C ₄₀	Al ₉ Fe ₂ Si ₂
AA6111		0.13%		

Figure 6 Thermo-Calc equilibrium phase fraction predictions for homogenization of AA6111 at 560°C (1040°F), based on the matrix composition of AA6111 given in Table 2.

Thermo-Calc predicts an additional phase, CrSi₂, in AA6111 + V where V can substitute for Cr and Al can substitute for Si. Since the Thermo-Calc database does not have the (Al,Zn)₁₈Mg₃(Cr,X)₂ phase, known as E phase (Figure 7), in its database for the Al-Mg-Cr system, it is likely that the CrSi₂ phase is equivalent to (Al,Zn)₁₈Mg₃(Cr,X)₂.

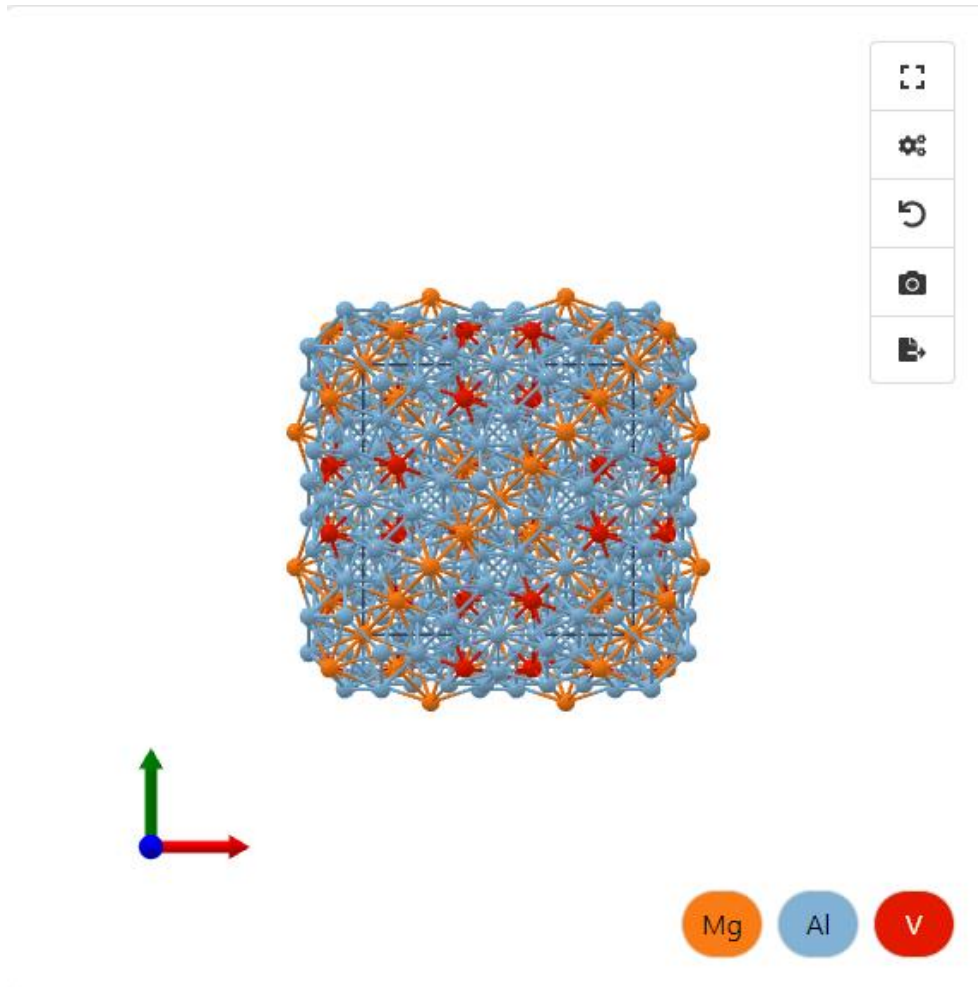
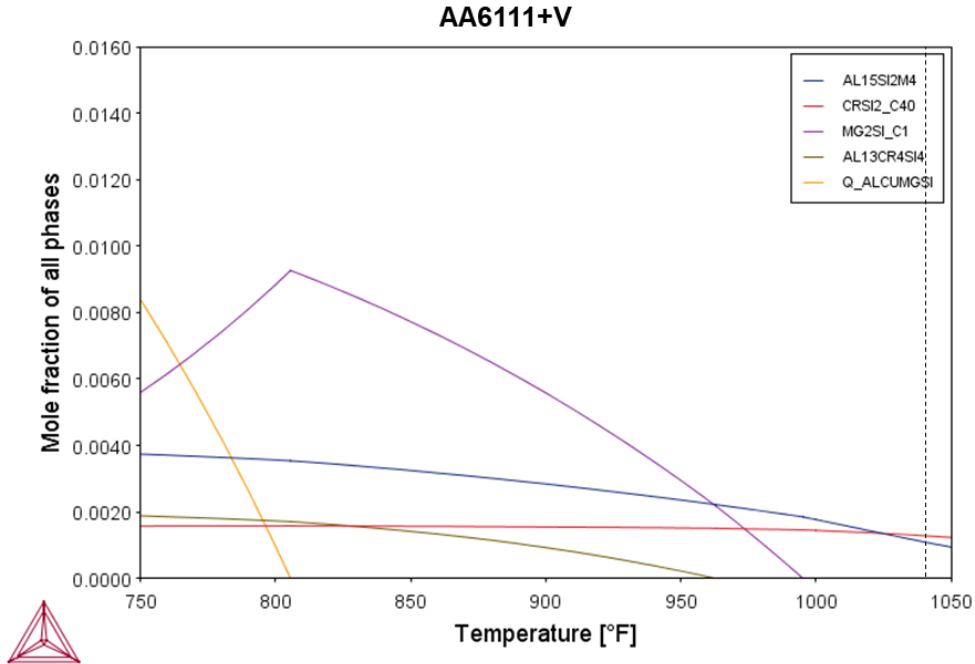


Figure 7 Crystal structure of α -Al₁₈Mg₃V₂ dispersoid. This dispersoid has a cubic structure, a space group Fd3m, 184 atoms in the unit cell, and a lattice parameter $a = 14.60\text{\AA}$ [13].

This phase is predicted to be an additional 0.13 mole percent dispersoid phase in AA6111+V (Figure 8).

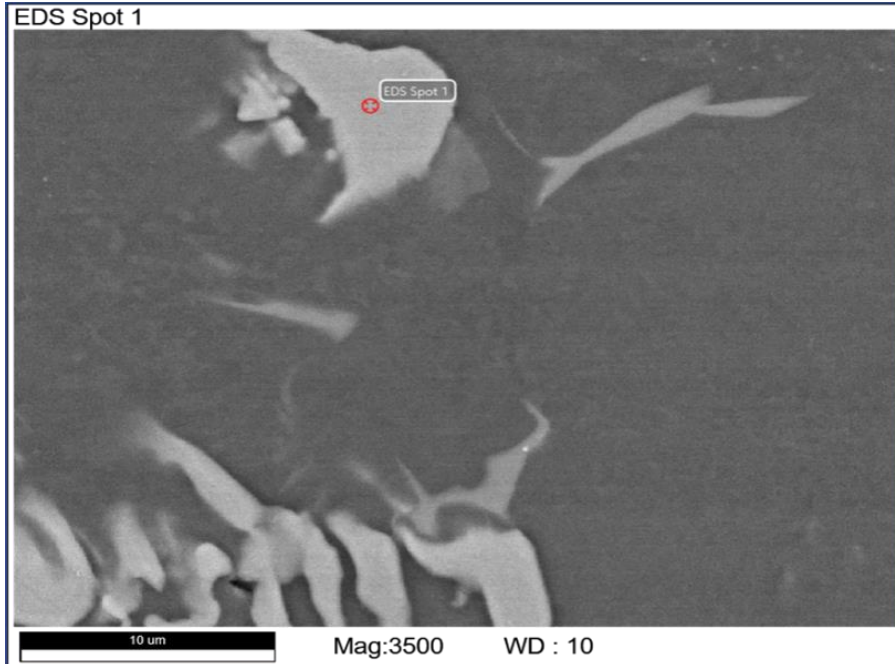


Equilibrium Phase Fraction at 560°C (1040°F) (mol %)				
Alloy	Al ₁₃ Cr ₄ Si ₄	Al ₁₅ Si ₂ M ₄	CrSi ₂ _C ₄₀	Al ₉ Fe ₂ Si ₂
AA6111 + V		0.11%	0.13%	

Figure 8 Thermo-Calc equilibrium phase fraction predictions for homogenization of AA6111 + V at 560°C (1040°F), based on the matrix composition of AA6111 + V given in Table 2.

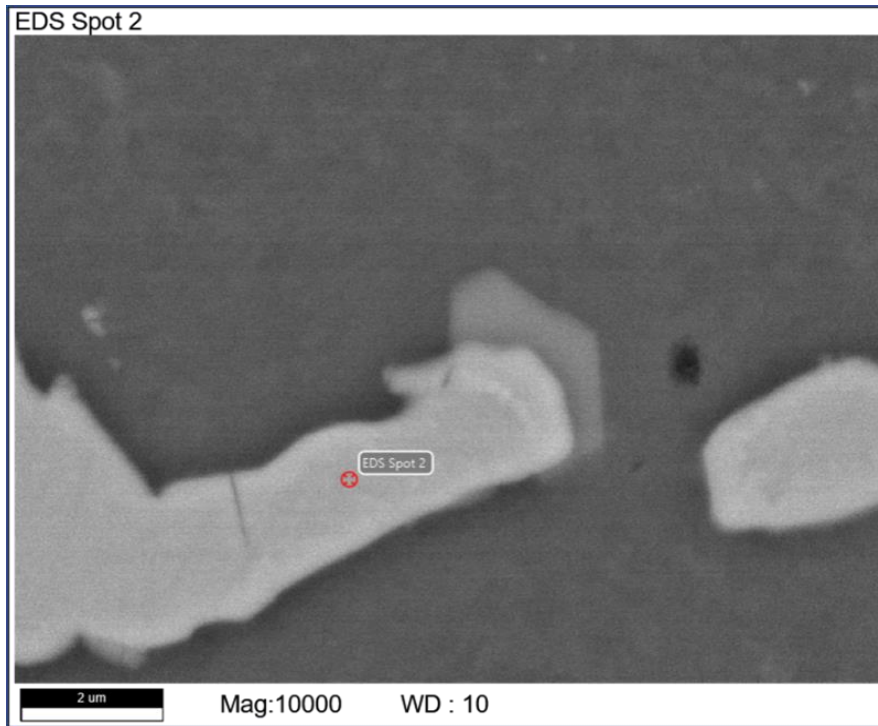
For these predictions it was determined that mole percent and volume percent are roughly equivalent for this alloy system.

Constituent and dispersoid phases were identified by a combination of x-ray diffraction Guinier analysis and SEM-EDS. EDS confirmed that there is one main constituent phase on the grain boundaries in both compositions. The main constituent phase that appears most prominently in both compositions contained Al, Fe, Mn, Si, and Cr and is likely to be the α -Al₁₂(Fe,Mn,X)₃Si phase (Figure 9) and in AA6111 + V in (Figure 10).



Element	Weight Percent	Atomic Percent
Aluminum	67.0	76.7
Silicon	9.3	10.2
Chromium	1.4	0.8
Manganese	5.4	3.1
Iron	14.3	7.9
Copper	2.6	1.3

Figure 9 SEM-EDS image suggesting the presence of α -Al₁₂(Fe,Mn,X)₃Si constituent in AA6111.



Element	Weight Percent	Atomic Percent
Aluminum	67.0	76.5
Silicon	9.9	10.8
Chromium	0.0	0.0
Manganese	6.2	3.5
Iron	14.0	7.7
Copper	2.9	1.4

Figure 10 SEM-EDS image suggesting the presence of α -Al₁₂(Fe,Mn,X)₃Si constituent in AA6111 + V.

Additionally, XRD indicated the presence of an additional phase in AA6111 + V (Figure 11), which is expected to be E-phase.

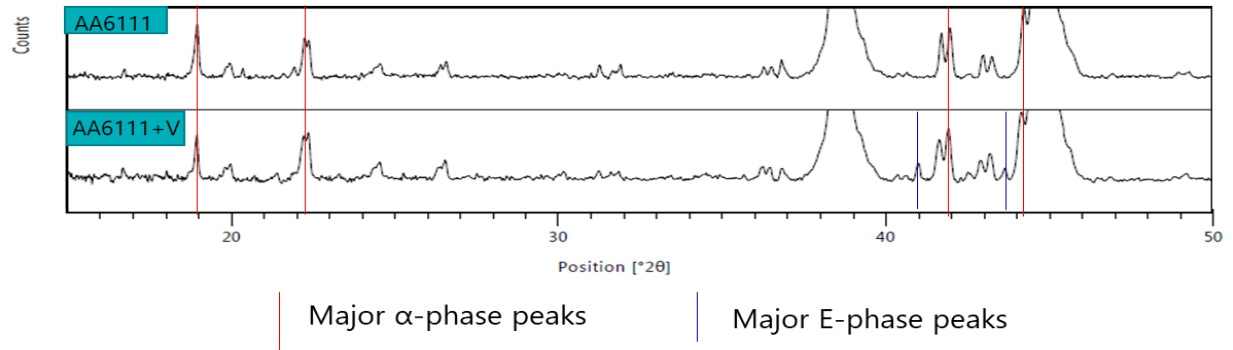


Figure 11 X-ray diffraction obtained from samples of AA6111 and AA6111 + V showing the various peaks. The large peaks at roughly 38.5° and 45° are the aluminum peaks and are present in both samples. The peaks present in both samples at roughly 19°, 20°, 22°, 25.5°, 27.5°, 31.5°, 36.5°, 42°, and 43° are the α - $\text{Al}_{12}(\text{Fe},\text{Mn},\text{X})_3\text{Si}$ peaks representing the constituent and dispersoid. The peaks at 41° and 43.5° in AA6111 + V, but not in AA6111 match two of the major E-phase peaks, however the minor E-phase peaks are not identifiable and the presence of E-phase cannot be confirmed with XRD.

SEM maps and SEM-EDS identified V in solid solution, as V-bearing constituent, and as V-bearing dispersoids which can be seen in Figure 12, Figure 13, and Figure 14 respectively.

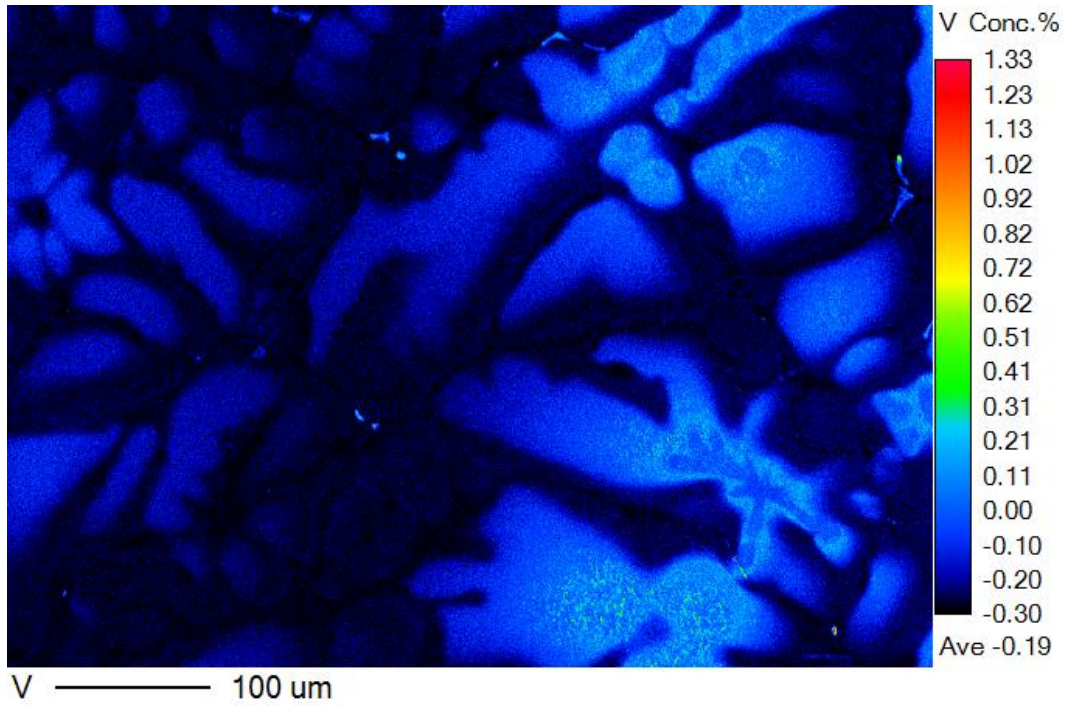
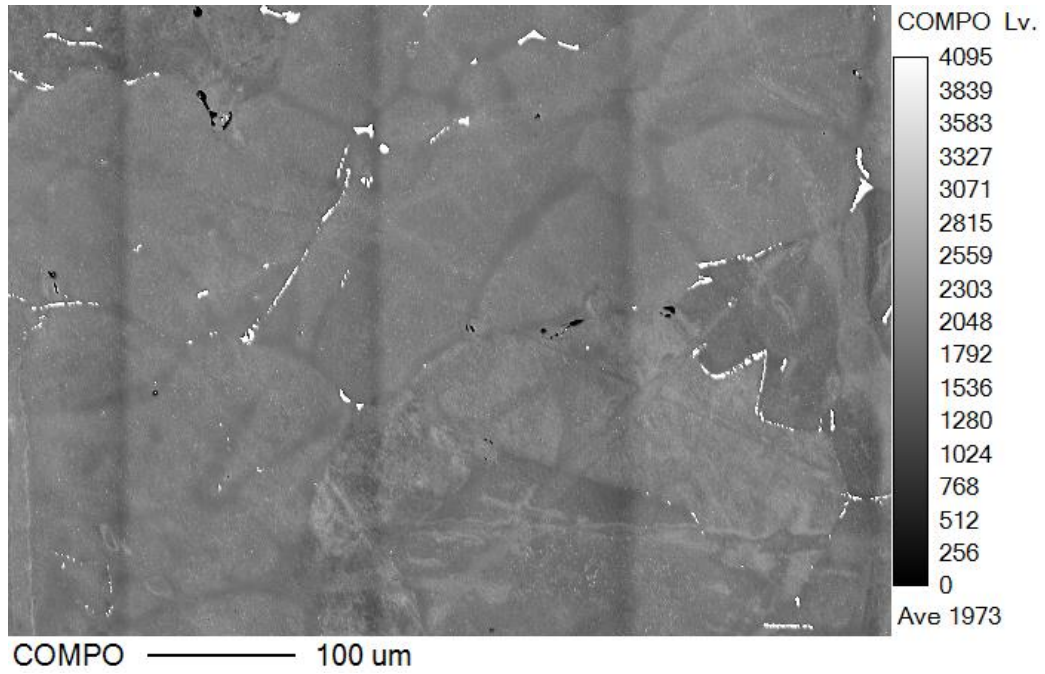
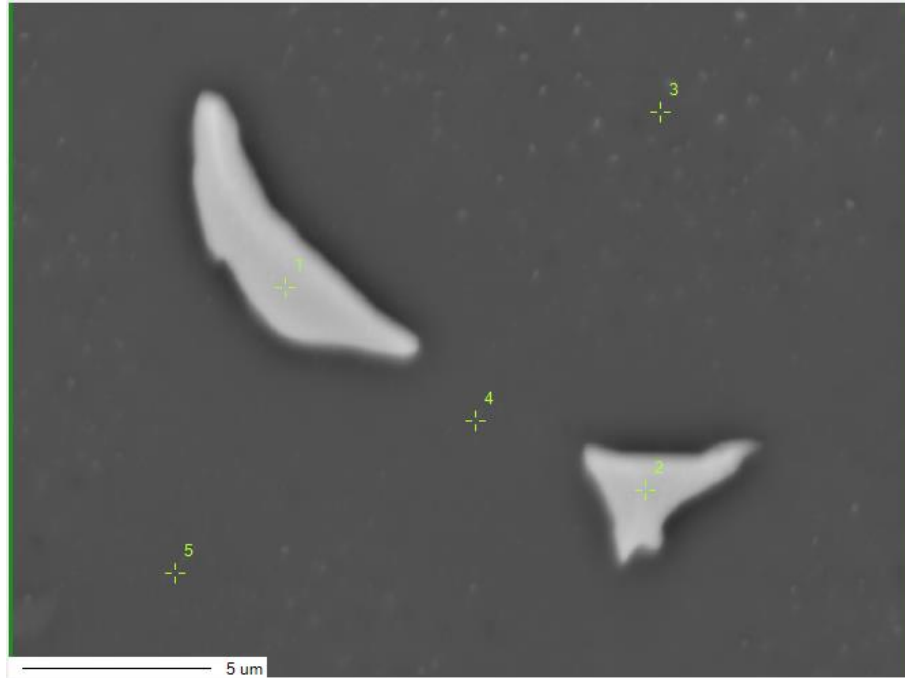


Figure 12 SEM map showing the presence of vanadium in grain interiors.



Elemental mass percent measured for spots 1-5								
	Al	Si	Mn	V	Cr	Fe	Cu	Mg
Spot 1	52.01	8.76	5.50	0.69	1.65	26.02	2.49	0.21
Spot 2	56.38	8.27	4.83	0.69	1.43	25.36	2.52	0.53
Spot 3	92.96	2.04	0.34	0.00	0.34	0.28	2.13	1.92
Spot 4	94.22	1.70	0.16	0.08	0.00	0.23	1.78	1.84
Spot 5	92.19	2.55	0.27	0.07	0.00	0.18	2.46	2.27

Figure 13 SEM-EDS showing the presence of V-bearing constituent on grain boundary.

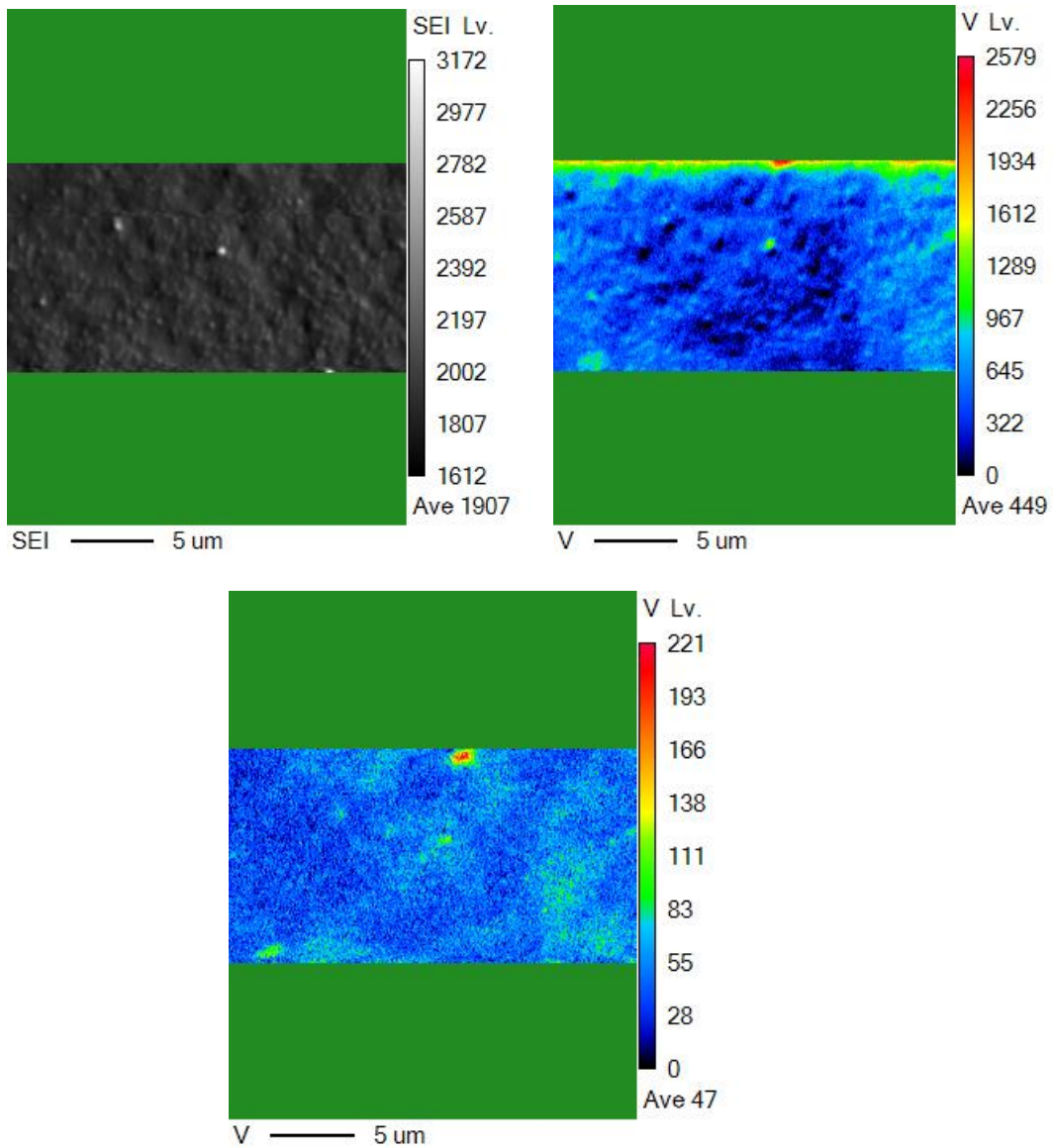


Figure 14 SEM map showing presence of V-bearing dispersoid particle.

Optical metallography was utilized to observe the dispersoid distribution in the 0.5% HF etched condition. Etch pits provide an indication of where the dispersoid particles are, even though the resolution of optical metallography is not sufficient to image the dispersoids themselves. For both compositions, it appears the dispersoid particles are less prevalent in the 2-hour homogenization condition than in the 24-hour homogenization condition, as expected.

Additionally, in both compositions a “cored” microstructure can be observed where the areas around the grain boundaries have no dispersoids. There are multiple explanations for this observation. First, this behavior could be due to solute partitioning during solidification. During solidification the elements which participate in a eutectic reaction with aluminum (Cu, Fe, Mn, Mg, Si) are concentrated in the grain boundary areas which are the last to solidify. Similarly, the elements which participate in a peritectic reaction with aluminum (Cr, V) are depleted in these regions, contributing to the “coring” behavior that is observed. Secondly, the “coring” behavior could be due to solute depletion because of constituent formation on the grain boundaries, leaving no dispersoid forming elements in solution in these areas. (Figure 15).

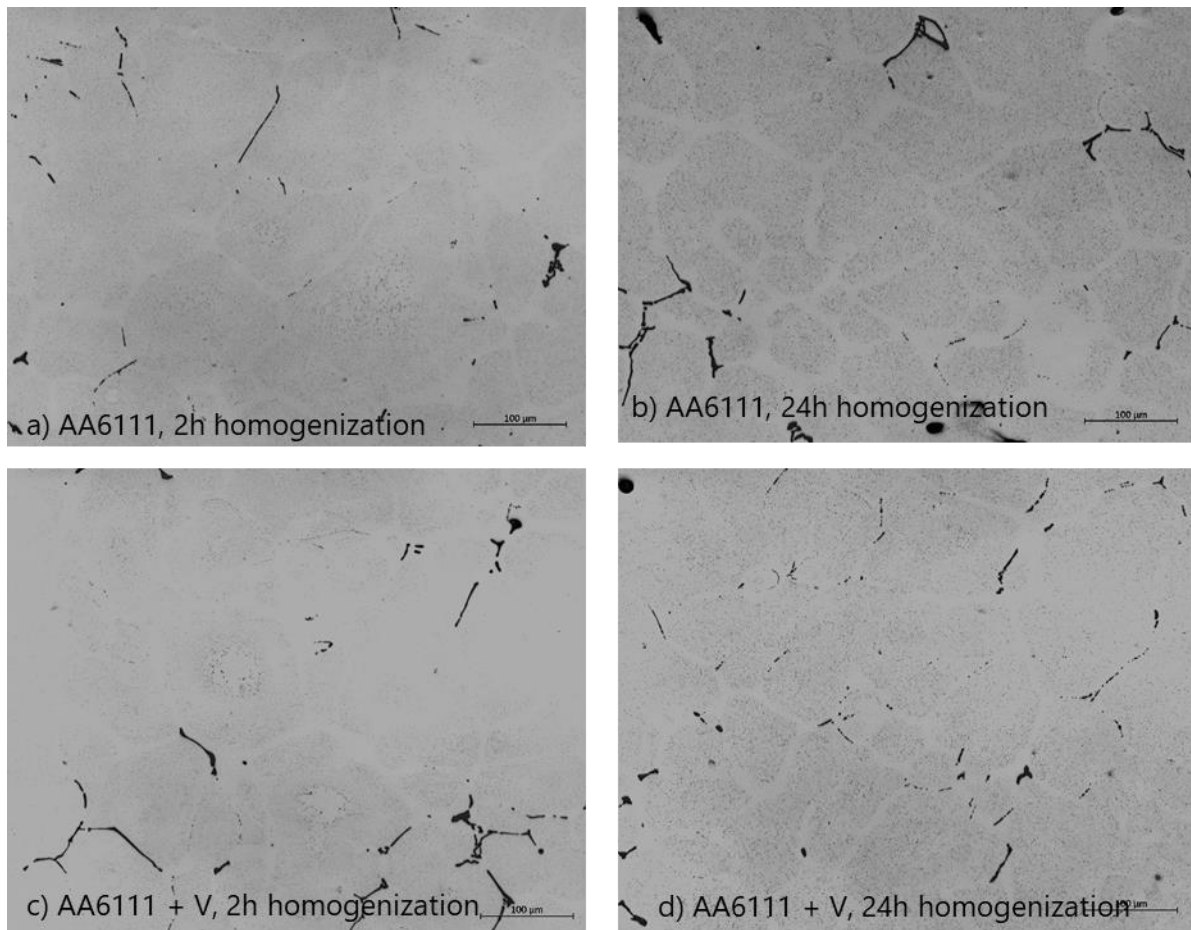


Figure 15 Optical metallography of (a, b) AA6111 and (c, d) AA6111 + V samples given (a, c) 2h and (b, d) 24 h homogenization practices, revealing etch pits associated with heterogenous dispersoid population.

Quantification of dispersoid particles was conducted on backscattered electron (BSE) images. An example BSE image used for this analysis can be seen in Figure 16.

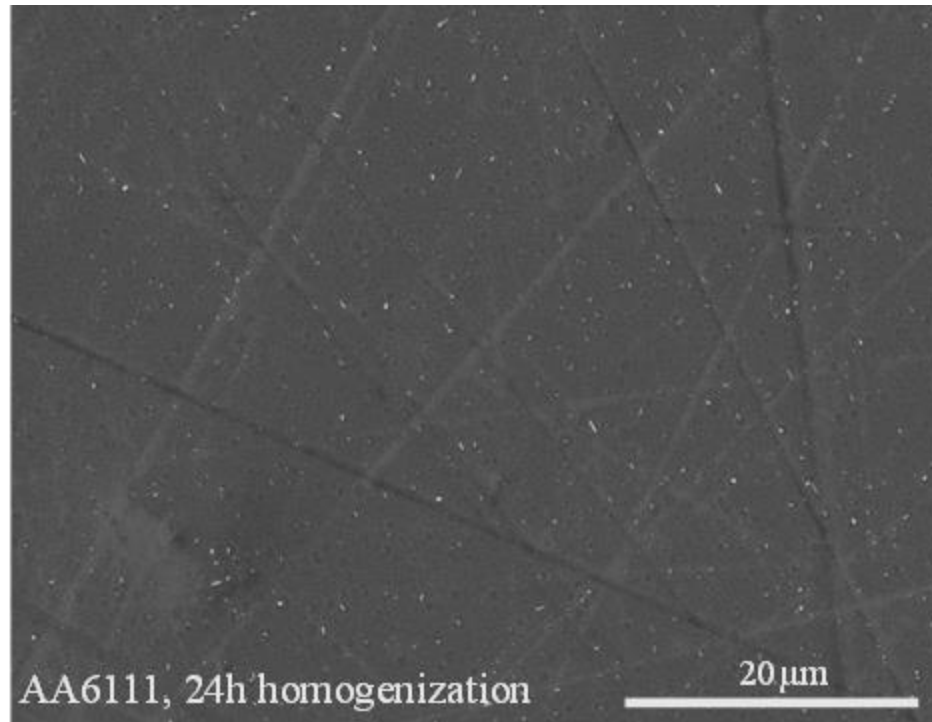


Figure 16 Representative SEM-BSE image from AA6111 with a 24-hour homogenization used for dispersoid quantification using ImageJ software.

Experimental measurements of the average dispersoid effective particle diameter in the base alloy, AA6111, were larger ($0.131\mu\text{m}$) for the 24-hour homogenization than for the 2-hour homogenization ($0.107\mu\text{m}$). Experimental measurements of the average dispersoid effective particle diameter in AA6111 + V were also larger ($0.131\mu\text{m}$) for the 24-hour homogenization than for the 2-hour homogenization ($0.099\mu\text{m}$) (Figure 17).

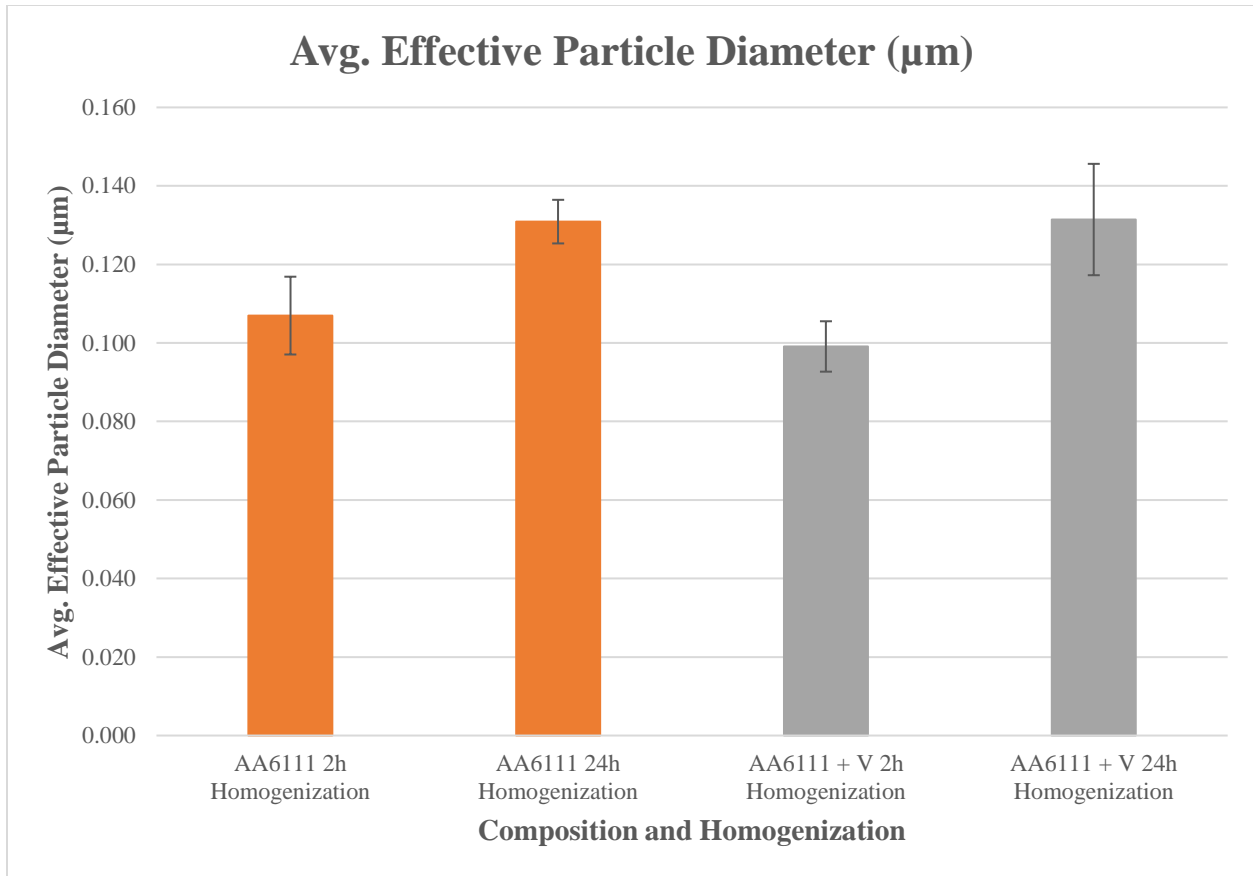


Figure 17 Average dispersoid effective particle diameter for the AA6111 and AA6111 + V given a 2-hour and 24-hour homogenization. Comparison shows a statistically significant difference in effective particle diameter within each alloy for the two different homogenization practices. Error bars reflect one standard deviation.

Additionally, experimental measurements of the area percent dispersoid in the base alloy AA6111 were slightly higher (0.612%) for the 24-hour homogenization than for the 2-hour homogenization (0.564%). Experimental measurements of the area percent dispersoid were also collected from AA6111 + V and the measurements were noticeably higher (0.694%) for the 24-hour homogenization versus the 2-hour homogenization (0.428%) (Figure 18).

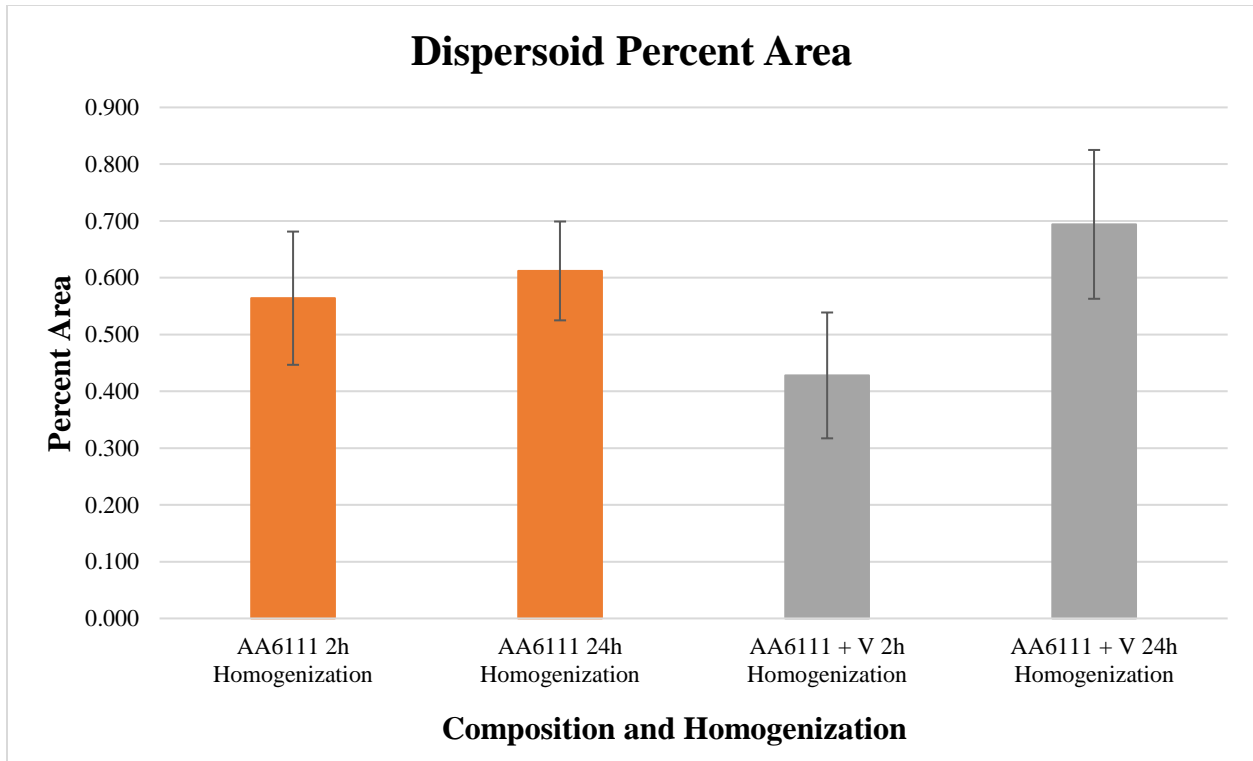


Figure 18 Comparison of total dispersoid percent area in AA6111 and AA6111 + V homogenized for 2-hours and 24-hours. Comparison shows a statistically significant increase in dispersoid percent area between AA6111 homogenized for 2-hours and 24-hours. Error bars reflect one standard deviation.

Effective dispersoid size, for this study measured as effective dispersoid diameter, was another key variable that was analyzed with respect to its effect on grain size and comparisons to what has been observed in the literature. According to the measurements shown in Figure 19 and Figure 20, the main average dispersoid population in both alloys and homogenizations is roughly 80 nanometers, with many of the dispersoids in the size range of 80 nm to 200 nm.

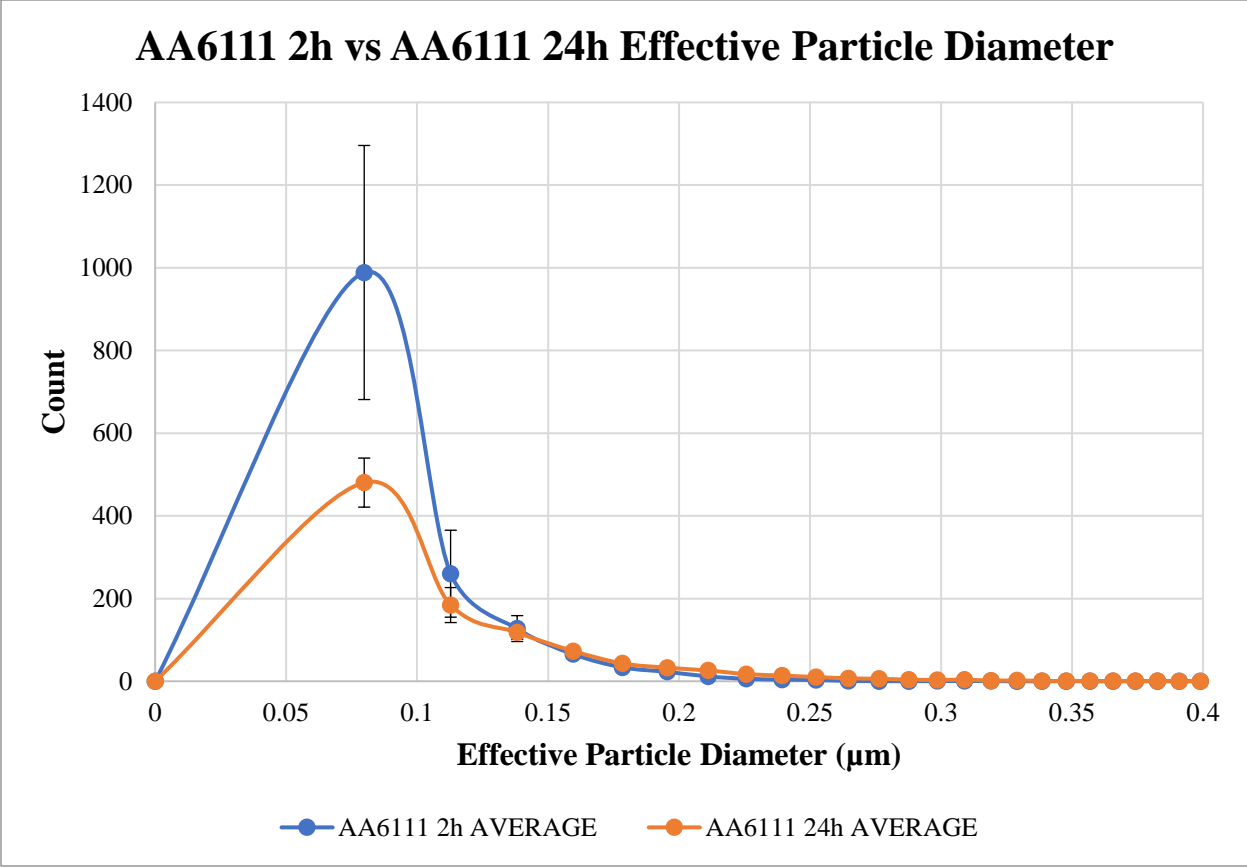


Figure 19 Histogram showing the amounts of particles measured in AA6111 when homogenized for 2-hours and 24-hours. Comparison shows both homogenizations yield similar particle size populations in differing amounts. Error bars reflect one standard deviation.

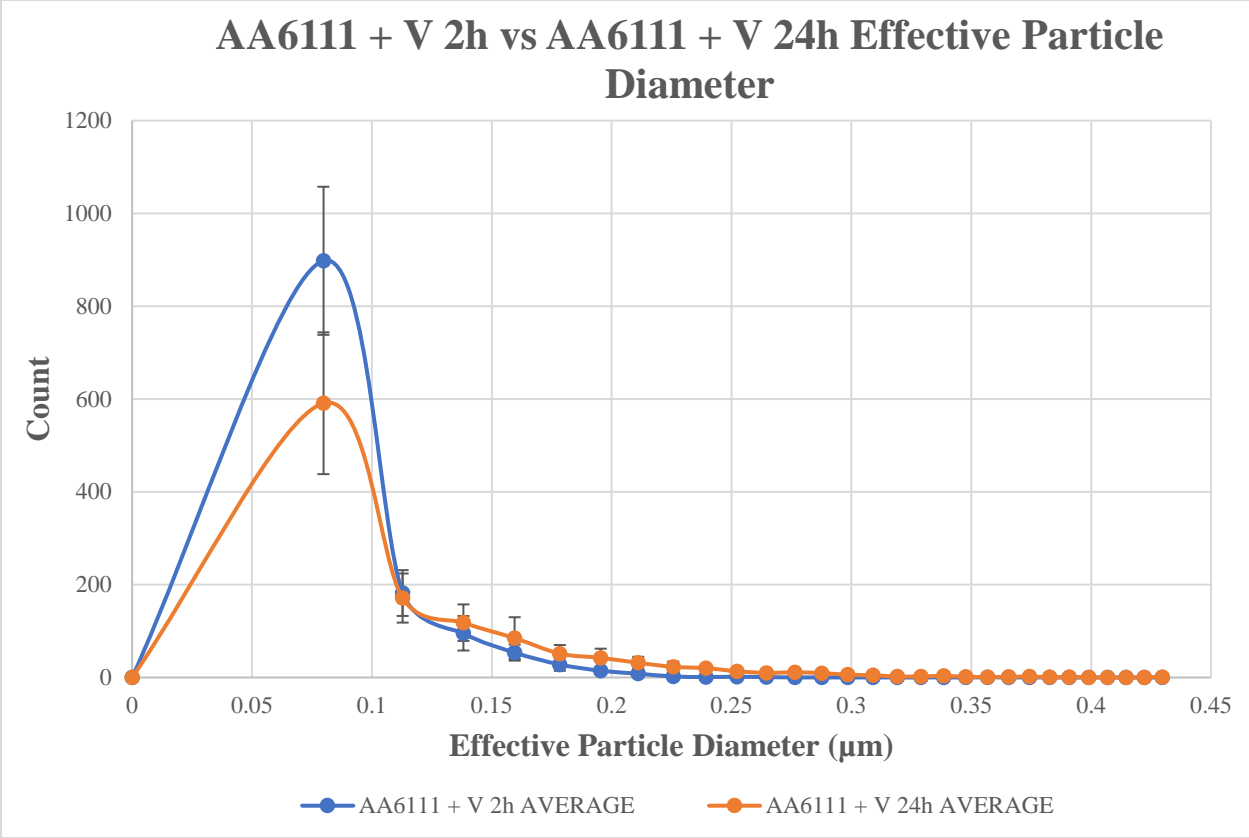


Figure 20 Histogram showing the amounts of particles measured in AA6111 + V when homogenized for 2-hours and 24-hours. Comparison shows both homogenizations yield similar particle size populations in differing amounts. Error bars reflect one standard deviation.

This size range is consistent with those reported in the literature where they evaluated dispersoids formed from Mn additions only [10] [18]. However, they did not provide histograms of the particle size distributions. In all conditions and compositions the longer 24-hour homogenization results in a slightly decreased grain size, independent of cold work percentage.

SEM-EBSD analysis was run to evaluate and compare area-weighted grain sizes as an effect of increased dispersoid grain pinning particles. For a given cold rolling reduction, increases in homogenization time led to slightly reduced grain size (Figure 21 and Figure 22, Table 4). In the case of 43% cold rolling reduction for the baseline alloy AA6111 and alloy AA6111 + V, grain

size was reduced from 53 to 51 μm and from 49 to 47 μm respectively (figure 21, Table 4). For 68% cold rolling reduction for the baseline alloy AA6111 and alloy AA6111 + V, grain size was reduced from 49 to 44 μm and from 45 to 42 μm , respectively (Figure 22, Table 4).

For a given homogenization time and level of cold rolling reduction, the impact of V was to reduce grain size. For example, in the case of 43% cold rolling reduction and 2-hour homogenization, the impact of V was to reduce grain size from 53 to 49 μm (Figure 21, Table 4). Similar reductions were observed for the longer homogenization time and for higher cold rolling reductions.

For both alloys and homogenization times, the grain size was reduced with higher levels of cold work. In the case of the baseline alloy AA6111, grain size was reduced from 53 μm to 49 μm when increasing cold rolling reduction from 43% to 68% for the 2-hour homogenization and from 51 μm to 44 μm when increasing cold rolling reduction from 43% to 68% for the 24-hour homogenization (Figure 21 and Figure 22, Table 4).

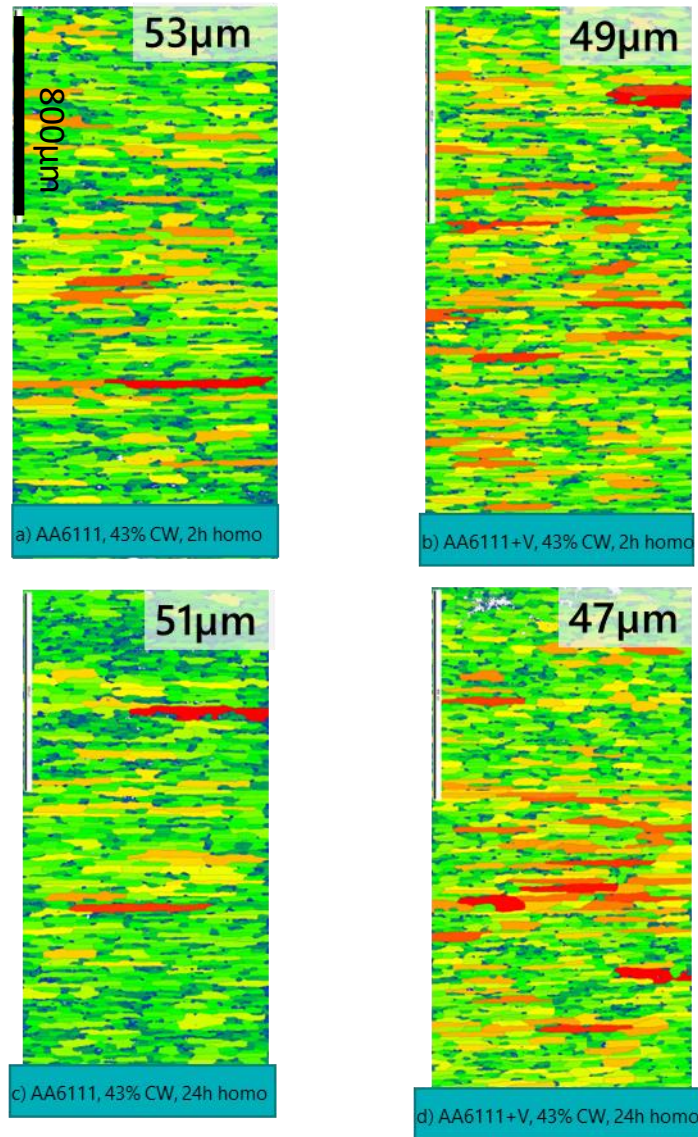


Figure 21 EBSD images of (a, c) AA6111 and (b, d) AA6111 + V samples all given 43% cold work reduction and (a, b) given 2-hour homogenization and (c, d) given 24-hour homogenization showing slight grain refinement with the addition of vanadium.

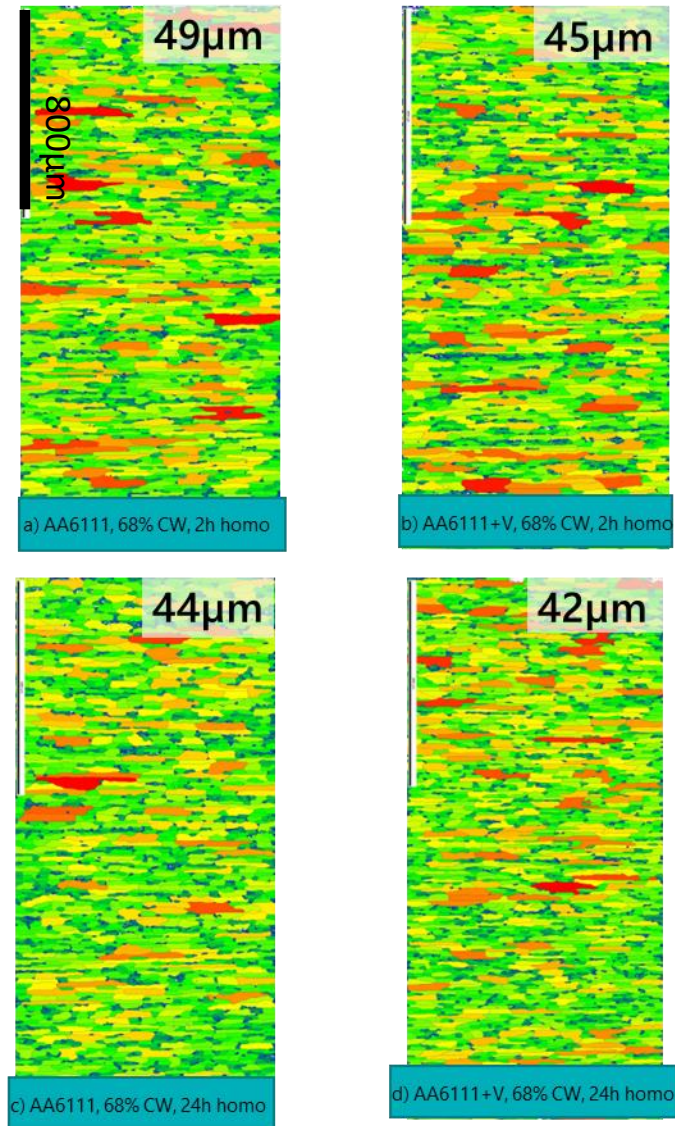


Figure 22 EBSD images of (a, c) AA6111 and (b, d) AA6111 + V samples all given 68% cold work reduction and (a, b) given 2-hour homogenization and (c, d) given 24-hour homogenization showing slight grain refinement with the addition of vanadium.

Likewise, for the alloy AA6111 + V, grain size was reduced from 49 μm to 45 μm when increasing cold rolling reduction from 43% to 68% for the 2-hour homogenization and from 47 μm to 42 μm when increasing cold rolling reduction from 43% to 68% for the 24-hour homogenization (Figure 21 and Figure 22, Table 4). Overall, the impact of increased homogenization time,

increased cold rolling reduction and the addition of V was to reduce the grain size. These effects were small but consistent across all comparisons.

Table 4 SEM-EBSD area-weighted grain size measurements for AA6111 and AA6111 + V given two homogenization treatments and two levels of cold work, then processed to T6 temper.

Alloy	Homogenization (h)	Percent cold work	Area weighted grain size
AA6111	2	43%	53
AA6111	2	68%	49
AA6111	24	43%	51
AA6111	24	68%	44
AA6111 + V	2	43%	49
AA6111 + V	2	68%	45
AA6111 + V	24	43%	47
AA6111 + V	24	68%	42

X-ray diffraction Guinier analysis identified significant amounts of the alpha phase, $Al_{12}(Fe,Mn)_3Si$ in both AA6111 and AA6111 + V. In AA6111 + V XRD detected small amounts of an additional phase that was not present in AA6111 (Figure 11). Additional peaks are observed at 41° and 43.5° in the XRD results for AA6111 + V, indicating the possibility of an additional phase. These two peaks match with two of E-phase's primary peaks, however this is not strong enough evidence to conclude that E-phase is present because the lower intensity peaks for E-phase were not observed.

Overall, the tensile results show no major impact with the addition of vanadium on the tensile yield strength (TYS), ultimate tensile strength (UTS), or total elongation with either

homogenization practice, cold work amount, or composition modification in the T4 or T6 temper (Table 5). In the T4 temper the TYS of AA6111 varied from 171 MPa to 178 MPa, UTS varied from 316 MPa to 322 MPa, and total elongation varied from 25.1% to 28.4% across the different homogenization practices and cold rolling reduction studies. Similarly, the TYS of AA6111 + V varied from 173 MPa to 180 MPa, UTS varied from 320 MPa to 324 MPa, and total elongations varied from 25.6% to 27.0%. Similar observations were made in the T6 temper. In the T6 temper the TYS of AA6111 varied from 365 MPa to 370 MPa, UTS varied from 388 MPa to 393 MPa, and total elongations varied from 9.8% to 12.8% across the different homogenization practices and cold rolling reductions studies. In the T6 temper the TYS of AA6111 + V varied from 368 MPa to 375 MPa, UTS varied from 394 MPa to 399 MPa, and total elongations varied from 9.5% to 12.7%. Differences of a few MPa may be within measurement error or expected lot-to-lot variation.

Table 5 Tensile test results for the AA6111 and AA6111 + V sheet, given two homogenization treatments and two levels of cold work, then processed to T4 and T6 tempers.

Alloy	Homogenization	Cold Work Percentage	Temper	TYS (Mpa)	UTS (MPa)	UTS-TYS	Uniform Elongation	Total Elongation	n-value (4-6%)	n-value (10-20%)
AA6111	2 hour	43%	T4	178	322	144	22.4	25.5	0.247	0.251
AA6111+V	2 hour	43%	T4	176	322	147	22.4	25.7	0.249	0.250
AA6111	2 hour	68%	T4	176	320	143.5	23.75	28.4	0.251	0.250
AA6111+V	2 hour	68%	T4	180	324	144	22.5	25.6	0.244	0.247
AA6111	24 hour	43%	T4	171	316	144	23.4	28.2	0.253	0.252
AA6111+V	24 hour	43%	T4	173	320	147	22.9	26.7	0.252	0.253
AA6111	24 hour	68%	T4	174	320	146	22.5	25.1	0.256	0.255
AA6111+V	24 hour	68%	T4	173	320	147	23.1	27.0	0.253	0.251
AA6111	2 hour	43%	T6	370	393	23	7.7	12.0	0.061	-
AA6111+V	2 hour	43%	T6	370	394	24	8.0	11.1	0.062	-
AA6111	2 hour	68%	T6	365	388	22	8.0	10.9	0.062	-
AA6111+V	2 hour	68%	T6	375	399	24.5	7.5	10.9	0.059	-
AA6111	24 hour	43%	T6	369	393	24	8.0	12.8	0.062	-
AA6111+V	24 hour	43%	T6	372	395	23.5	7.0	9.5	0.060	-
AA6111	24 hour	68%	T6	369	392	23	7.5	9.8	0.062	-
AA6111+V	24 hour	68%	T6	368	394	26	8.2	12.7	0.063	-

Overall, there was no impact on n-value with either homogenization practice, cold work amount, or composition modifications in the T4 or T6 temper (Figure 23 and Figure 24). The strain hardening exponent (n-value) evaluated over the strain range from 4 to 6% varied from 0.247 to 0.256 in the T4 temper and 0.061 to 0.062 in the T6 temper in AA6111. Similarly, the 4-6% strain hardening exponent (n-value) varied from 0.244 to 0.253 in the T4 temper and 0.059 to 0.063 in the T6 temper of AA6111 + V.

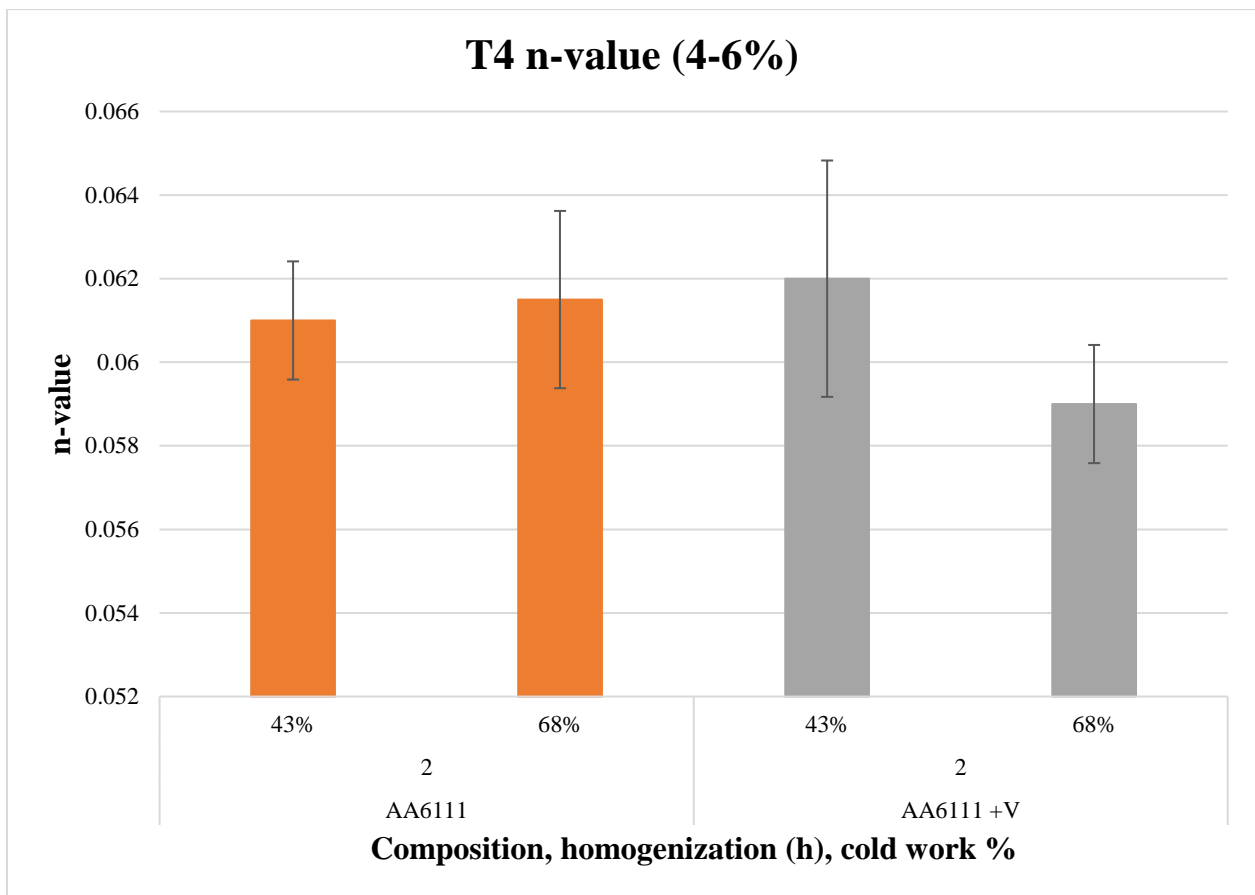


Figure 23 Comparison of the n-value (4-6%) of AA6111 and AA6111 + V given a 2-hour homogenization, 43% and 68% cold work reductions, and aged to the T4 condition. Values show no significant benefit to n-value by adding vanadium to AA6111. Error bars reflect one standard deviation.

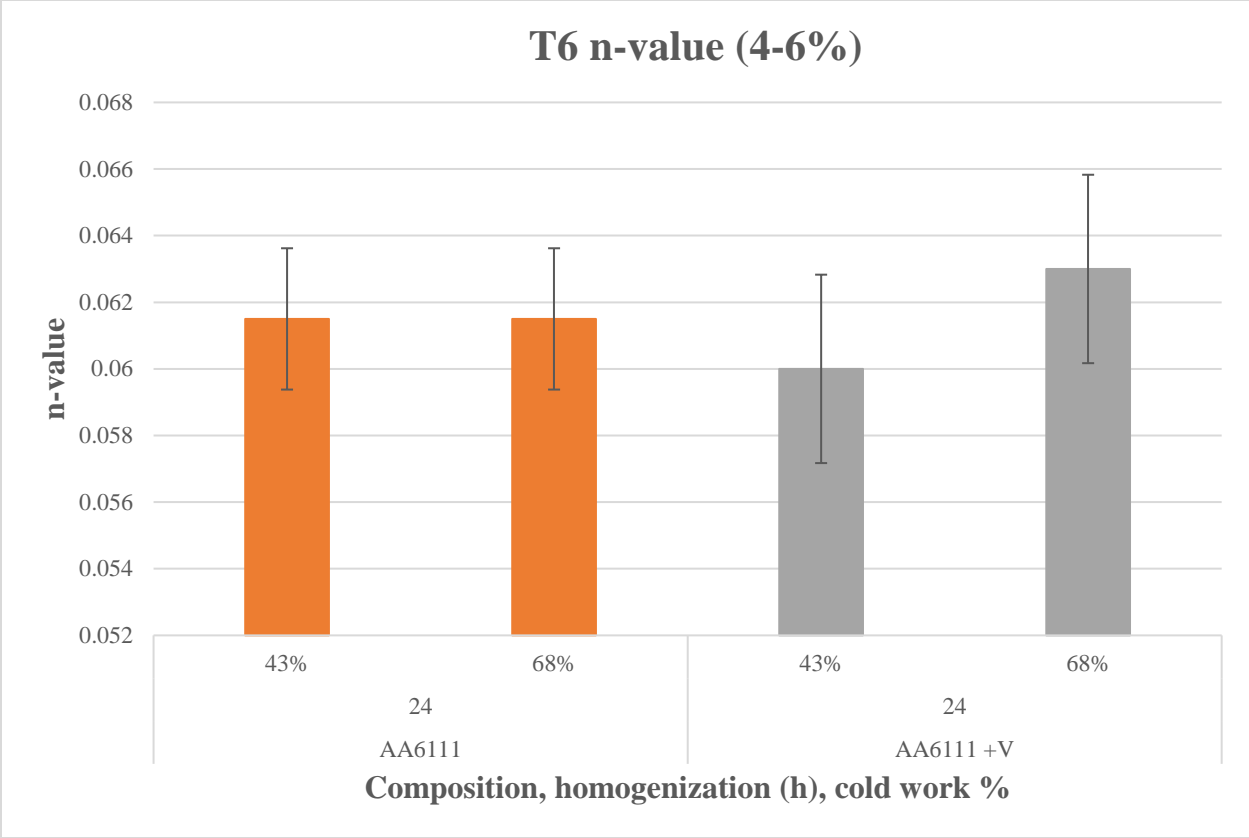


Figure 24 Comparison of the n-value (4-6%) of AA6111 and AA6111 + V given a 24-hour homogenization, 43% and 68% cold work reductions, and aged to the T6 condition. Values show no significant benefit to n-value by adding vanadium to AA6111. Error bars reflect one standard deviation.

5.0 Discussion

The size, amount, and distribution of dispersoid particles in 6xxx series aluminum alloys plays an integral role in the resulting microstructure. Studying the effect of adding an additional dispersoid forming element to a known automotive composition to evaluate the resulting microstructure and properties showed some positive impact on grain size reduction, but overall had minimal effect on performance.

Thermo-Calc was used to predict phase formation during solidification and equilibrium. Thermo-Calc predicted the formation of an additional dispersoid phase with the addition of vanadium and use of a 560°C homogenization. The prediction of this additional phase and overall greater phase fraction in the AA6111 + V composition led to interest of the impact on microstructure and properties.

Thermo-Calc predictions can be seen for AA6111 in Figure 7 and AA6111 + V in Figure 8. Thermo-Calc uses a public database for its predictions, which means there is a possibility for different notations for different phases. For example, Thermo-Calc predicts $\text{Al}_{15}\text{Si}_2\text{M}_4$ as this is the standard alpha phase in the database for the Al-Mn-Si ternary system. Upon further evaluation using SEM-EDS and XRD, this phase was assumed to be $\alpha\text{-Al}_{12}(\text{Fe},\text{Mn},\text{Cr})_3\text{Si}$. Additionally, Thermo-Calc predicts that an additional dispersoid phase, CrSi_2 , will be present in AA6111 + V. Due to the differences in the phase notations, Thermo-Calc does not have E phase, $\text{Al}_{18}\text{Mg}_3\text{V}_2$, in the Al-Mg-Cr ternary system. Instead, it has a phase called CrSi_2 where V can substitute for Cr and Al can substitute for Si. Since Thermo-Calc does not have the E-phase in the Al-Mg-Cr system it is likely these are equivalent phases. Predictions for both alloys show $\text{Al}_{15}\text{Si}_2\text{M}_4$ dispersoid phase. Precedence from the literature by Lodgaard and Ryum, suggests that this phase is an α -

Al(Mn,Cr,Fe)Si dispersoid [18]. XRD analysis also confirmed this phase to be α -Al₁₂(Fe,Mn)₃Si. Additionally, XRD analysis identified two additional peaks in AA6111 + V that match two of E-phase's major peaks.

Homogenization time played a significant role in the resulting distribution of dispersoids for both compositions. Figure 18 shows the measured dispersoid percent areas as a function of composition and homogenization time. For AA6111 these measurements show that a 2-hour homogenization at 560°C is sufficient to reach equilibrium and there is no significant increase in the amount of dispersoid area with the 24-hour homogenization. However, these measurements also show that for AA6111 + V there is a significant increase in the dispersoid amount with the 24-hour homogenization. The results observed here make sense given the different dispersoid forming elements that are involved. Both compositions rely on Mn diffusion during homogenization to form dispersoids but AA6111 + V is also impacted by V diffusion. The diffusion coefficient of manganese in aluminum at 560°C is $7.42 \times 10^{-16} \text{ m}^2/\text{s}$, while the diffusion coefficient of vanadium in aluminum at 560°C is $1.73 \times 10^{-19} \text{ m}^2/\text{s}$ [8]. Since manganese is a much faster diffusing element in aluminum, the results show that the manganese diffusion and precipitation of dispersoids in AA6111 reaches or almost fully reaches equilibrium with a 2-hour homogenization. Conversely, the dispersoid percent area results for AA6111 + V show a significant increase in dispersoid area with a 24-hour homogenization. These results are also consistent with the fact that vanadium is a much slower diffusing element in aluminum. The longer homogenization practice allows additional time for the vanadium to diffuse and the dispersoids to precipitate, resulting in an increase in dispersoid percent area.

Not surprisingly, the increased cold rolling reduction successfully reduced the grain size. In every condition (different homogenization times and different cold work levels), the addition of

vanadium appears to produce a slightly finer grain size than traditional AA6111. However, there was no observed difference in particle morphology or a clear distinction in size distribution between the $\alpha\text{-Al}_{12}(\text{Fe,Mn,X})_3\text{Si}$ dispersoid and the additional dispersoid formed. Furthermore, SEM-EDS was able to identify a vanadium-bearing dispersoid particle, but they were less prevalent than expected. There are multiple explanations for why the vanadium-bearing dispersoids were not easily identified by SEM-EDS. First, it is possible that the 24-hour homogenization was not long enough for the vanadium to diffuse and form large amounts of E-phase. Since vanadium is such a slow diffuser in aluminum, it is possible that a 24-hour homogenization was simply insufficient. Second, the vanadium could have diffused and substituted into the $\alpha\text{-Al}_{12}(\text{Fe,Mn,X})_3\text{Si}$ phase where vanadium substitutes in for X. In this case it is likely there would be no difference in size or morphology of the dispersoid particles and may be difficult to identify using SEM-EDS. It may be that SEM-EDS does not have sufficient resolution to adequately identify the small vanadium-bearing dispersoids, but a technique such as transmission electron microscopy (TEM) could more effectively identify and quantify these dispersoids. Based on the similar dispersoid area percents measured for both alloys, it is fair to assume AA6111 + V contains mostly $\alpha\text{-Al}_{12}(\text{Fe,Mn,X})_3\text{Si}$ with a smaller population of an additional dispersoid phase seen in the longer homogenization. Understanding this, the addition of vanadium resulted in a slightly reduced grain size in all conditions compared to AA6111.

The concept of Zener drag, or Zener pinning, likely contributed to the slightly refined grain sizes with vanadium additions [19]. Zener drag is the idea that the smaller the spacing between dispersed second phase particles, the smaller the expected grain size [11]. Smaller interparticle spacings are realized with either higher amounts of particles or reductions in the size of those particles. This experiment attempted to compare a 2-hour and 24-hour homogenization of two

alloys with different amounts of dispersoid forming elements and evaluate if the addition of vanadium would have a significant effect on Zener drag, thus producing a finer grain size. These particles act as barriers for grain boundary motion. When grain boundaries encounter these particles, new grain boundary area must be created which requires a much higher energy state. Since this process is energetically unfavorable, it is an effective method of pinning grain boundary movement which has a large influence on recovery, recrystallization, and grain growth [11]. One way to plot the Zener drag effect is to plot grain size as a function of f/r , where f is the fraction of dispersoid particles (area percent divided by 100), and r is particle radius. This calculation was completed to analyze the effect of Zener pinning in AA6111 and AA6111 + V and the results can be seen in Figure 25.

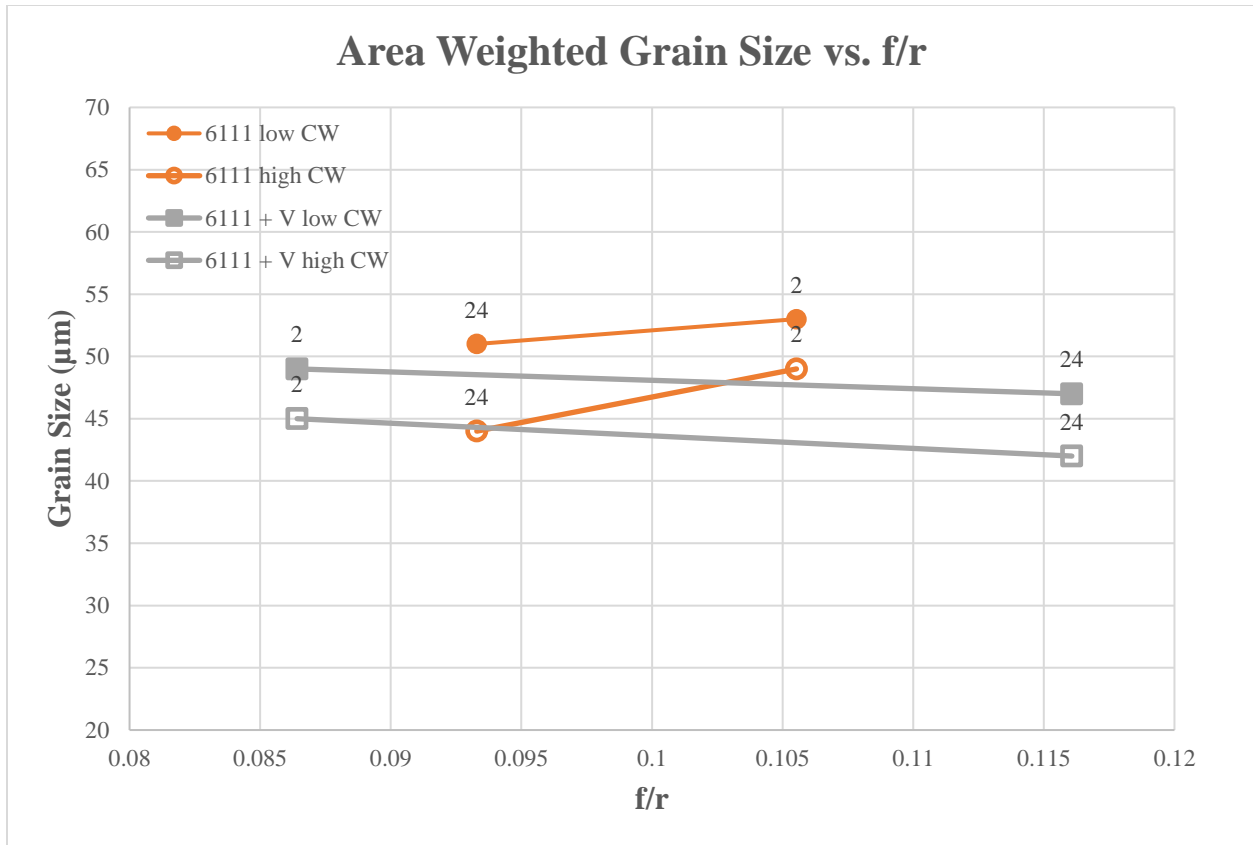


Figure 25 Area weighted grain size versus f/r parameter for both compositions, homogenization times, and cold work levels. The f/r parameter provides a representation of Zener drag in the material. The baseline AA6111 material does not follow the expected result that an increase in f/r value should increase the Zener drag effect and decrease grain size. AA6111 + V does follow the expected trend.

AA6111 + V follows the expected trend where grain size decreases with increasing f/r. This can be explained by the formation of an additional dispersoid phase with vanadium additions, creating more pinning particles. However, the baseline AA6111 does not follow the expected trend. One possible explanation for this could be that a 2-hour homogenization is sufficient to form the equilibrium amount of $\alpha\text{-Al}_{12}(\text{Fe},\text{Mn},\text{X})_3\text{Si}$ dispersoids. When this material is given a 24-hour homogenization, there is no additional phase or additional $\alpha\text{-Al}_{12}(\text{Fe},\text{Mn},\text{X})_3\text{Si}$ being formed. Increasing particle radius via particle coarsening with no change in f leads to a decrease in f/r with

increased homogenization time. In AA6111 + V, the 2-hour homogenization is sufficient to begin forming $\alpha\text{-Al}_{12}(\text{Fe,Mn,X})_3\text{Si}$ dispersoids, but does not form much, if any, vanadium-bearing phase due to the slow diffusion rate of vanadium. The 24-hour homogenization results in a significant increase in dispersoid percent area, which in turn increases the value of f . Even though the average radius of the particles is statistically the same for both alloys in each homogenized condition (Figure 17), this increase in f for AA6111 + V, but not AA6111 is the reason why AA6111 + V follows the expected f/r prediction but AA6111 does not. It is fair to conclude that the larger increase in dispersoid area was able to be captured in the particle measurements for AA6111 + V, but since the dispersoid percent areas were so similar in the 2-hour and 24-hour homogenizations for AA6111, the differences were not distinguishable in the dispersoid measurements.

5.1 Mechanical Properties

The manipulation of the dispersoid populations in AA6111 and AA6111 + V had no significant improvement in T4 or T6 strength, n -value, UTS-TYS, or elongation. While there is precedence in the literature stating that vanadium additions to 6xxx series aluminum alloys improves the mechanical properties, that was not observed in this study [4] [14] [15] [16] [20]. No additional strength benefit from these dispersoids is not surprising. There are two main strengthening mechanisms that could potentially be affected by the amount of dispersoids present: dispersion strengthening and grain size strengthening. First is the contribution that could come from dispersion strengthening, i.e., Orowan looping. In 6xxx series aluminum the main strength contribution comes from aging the material and precipitating out β'' and Q' particles. A paper by Wang *et al.*, 2013 examined these strengthening particles in AA6111 in the T6 temper. These

particles are much smaller (~1-3nm radius) and appear in large number densities (75 to 200 x 10³/μm³ for β'' and 1 to 4 x 10³/μm³ for Q') [24]. The Orowan looping mechanism can provide additional strengthening when small particles act as barriers to dislocation motion and cause the dislocations to shear or bypass the particles. When compared to the much larger 50-65nm radius of the dispersoids the expected increase in strength from the dispersoid precipitates is negligible.

Additionally, little to no strength benefit is expected in these alloys due to a more refined grain size in AA6111 + V. The Hall-Petch equation is based on the theory of grain boundary strengthening. Grain boundaries act as pinning locations for dislocation movement. With a more refined grain size, there is more grain boundary area, which in theory should help increase the strength of the material. The Hall-Petch equation is defined as:

$$\sigma_y = \sigma_0 + k_y d^{-1/2} \quad (5-1)$$

where d is the average grain diameter and σ₀ and k_y are material specific constants [5]. Based on this equation, strength should increase with decreasing grain size. Figure 26 shows yield strength data compiled by *Burger et al., 1995* of a 6xxx series aluminum alloy in the T4 temper. This study did not show an increase in strength for samples whose grain size varied from about 27 to 46μm. Although the data show what appears to be a slight decrease in strength with reductions in grain size, *Burger et al., 1995* explain that the slope of the trend line is not statistically significant from zero, indicating no strength increase in strength is observed over the grain size range plotted. Based on this data we would not expect to see a notable increase in strength associated with a reduction in grain size from 51 to 42μm as observed in the AA6111 and AA6111 + V samples in the current study.

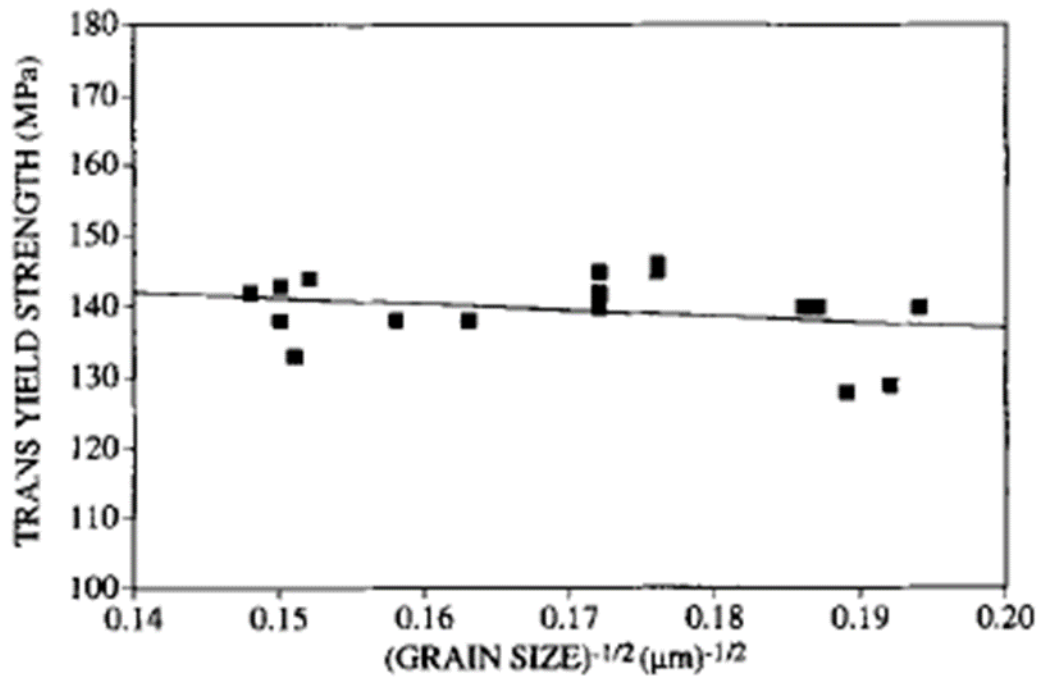


FIG. 17. Variation of yield stress with grain size in a 6000 series alloy in T4 temper.

Figure 26 Yield strength variation in a 6xxx series aluminum alloy in the T4 temper compiled by Burger et al., 1995. The slope of the trendline was found to not be statistically significant from zero, indicating no strength increase due to grain size reduction from 46 to 27μm [6].

6.0 Conclusions

This study provided a detailed analysis of the effects of vanadium additions to the aluminum automotive alloy AA6111. Based on this investigation there are multiple conclusions that can be made.

The addition of vanadium resulted in slight grain a slight grain refinement of 2-4 μ m depending on the processing path. All samples showed a fully recrystallized grain structure in the T4 and T6 temper as expected.

SEM evaluation identified the presence of vanadium in multiple locations in the microstructure. Even after a 24-hour homogenization treatment, SEM identified much of the vanadium in the grain interiors, suggesting the 24-hour homogenization was still insufficient for the vanadium to diffuse and reach an equilibrium state. SEM also identified vanadium in constituent particles suggesting some vanadium was tied up in these particles during the solidification process. SEM did identify a vanadium-bearing dispersoid particle, however these particles were not as prevalent as expected or the resolution of the SEM was not quite high enough to identify these particles.

The vanadium additions did not result in measurable increases to either the tensile yield strength or the ultimate tensile strength. The main strengthening mechanisms in aluminum alloys were discussed and based on these strengthening mechanisms it is not surprising that no increase was observed.

The vanadium additions showed no measurable improvements in either total elongation or n-value. It was hypothesized that an increase in dispersoid particles could help more uniformly

distribute strain and this would be evident through increased total elongations and n-value, however this was not observed in this study.

7.0 Recommendation and Future Work

Overall, the addition of vanadium to the automotive alloy AA6111 yielded a slightly finer grain size but did not have an impact on tensile yield strength, ultimate tensile strength, elongation, or n-value. The longer 24-hour homogenization was sufficient for some vanadium diffusion and precipitation of a vanadium-bearing dispersoid phase which slightly refined the grain size in this alloy. Although the addition of vanadium presents the benefit of slightly refining grain size, the effect is so small that no other performance benefits were observed. The use of vanadium may not be a realistic recommendation for improving AA6111, especially in production where the residual vanadium content would be harmful to the reuse of scrap material.

Further study on the effect of vanadium in solid solution could provide important additional information on the role vanadium plays in aluminum alloys. A full natural aging curve could be compiled to study the effect of vanadium on the precipitation kinetics of the strengthening phases when vanadium is present in solid solution.

Thin foil TEM could be conducted on the 24-hour homogenized samples from this study to characterize and quantify the vanadium-bearing dispersoid formed. Additionally, longer homogenization treatments could be designed and tested to evaluate the impact on E-phase formation and alloy performance.

New alloy investigation could minimize the amount of other dispersoid forming elements, namely manganese and chromium, to solely evaluate the behavior of vanadium in a 6xxx series aluminum alloy and its impact on performance. Formability testing could be included to determine if that aspect of performance is affected.

Bibliography

- [1] Aluminum Alloys 101. (2020). Retrieved from <https://aluminum.org/resources/industry-standards/aluminum-alloys-101>
- [2] American National Standard Alloy and Temper Designation Systems for Aluminum, H351./H35.1(M), The Aluminum Association, 2017 edition, (May 12, 2017).
- [3] *Appendix 1 Crystal Structure Descriptions*. (2009).
- [4] Boczkal, S., Lech-Grega, M., Morgiel, J., & Piela, K. (2014). Effect of Vanadium Additions on the Structure of Aluminium (Al99.5) and 6xxx Aluminium Alloys. In *Light Metals 2014* (Vol. 9781118889084, pp. 261–264). Wiley Blackwell. <https://doi.org/10.1002/9781118888438.ch45>
- [5] Burger, G.B., Gupta, A.K., Jeffrey, P.W., & Lloyd, D.J. (1995). Microstructural Control of Aluminum Sheet Used in Automotive Applications. *Materials Characterization* 35:23-39.
- [6] Callister Jr., W. D., & Rethwisch, D. G. (2010). *Materials Science and Engineering An Introduction* (Eighth Edition).
- [7] Djukanovic, G. (2019, February 28). Aluminium Alloys in the Automotive Industry: a Handy Guide. Retrieved from <https://aluminiuminsider.com/aluminium-alloys-automotive-industry-handy-guide/>
- [8] Du, Y., Chang, Y. A., Huang, B., Gong, W., Jin, Z., Xu, H., Yuan, Z., Liu, Y., He, Y., & Xie, F. Y. (2003). Diffusion coefficients of some solutes in fcc and liquid Al: Critical evaluation and correlation. *Materials Science and Engineering A*, 363(1–2), 140–151. [https://doi.org/10.1016/S0921-5093\(03\)00624-5](https://doi.org/10.1016/S0921-5093(03)00624-5)

- [9] Hatch, J. E. (1984). *Aluminum Properties and Physical Metallurgy*. American Society for Metals.
- [10] Hu, R., Ogura, T., Tezuka, H., Sato, T., & Liu, Q. (2010). Dispersoid formation and recrystallization behavior in an Al-Mg-Si-Mn alloy. *Journal of Materials Science and Technology*, 26(3), 237–243. [https://doi.org/10.1016/S1005-0302\(10\)60040-0](https://doi.org/10.1016/S1005-0302(10)60040-0)
- [11] Hunderi, O., Nes, E., & Ryum, N. (1989). ON THE ZENER DRAG – ADDENDUM. *Acta metal.* Vol. 37, No. 1, pp. 129-133.
- [12] Hurlbut, C.S., Klein, C. (1977). *Manual of Mineralogy, 9th Edition*. John Wiley and Sons, New York.
- [13] Jain, A., Ong, S. P., Hautier, G., Chen, W., Richards, W. D., Dacek, S., Cholia, S., Gunter, D., Skinner, D., Ceder, G., & Persson, K. A. (2013). Commentary: The materials project: A materials genome approach to accelerating materials innovation. In *APL Materials* (Vol. 1, Issue 1). American Institute of Physics Inc. <https://doi.org/10.1063/1.4812323>
- [14] Kumar, A., & Sasikumar, C. (2017). Effect of Vanadium addition to Al-Si alloy on its mechanical, tribological and microstructure properties. In *Materials Today: Proceedings* (Vol. 4). www.sciencedirect.com/www.materialstoday.com/proceedings
- [15] Lech-Grega, M., Szymański, W., Boczekal, S., Gawlik, M., & Bigaj, M. (2015). *THE EFFECT OF VANADIUM ADDITION ON STRUCTURE AND MATERIAL PROPERTIES OF HEAT TREATED 6XXX SERIES ALUMINIUM ALLOYS*.
- [16] Lech-Grega, M., Szymański, W., Gawlik, M., & Bigaj, M. (2012). *HOMOGENIZATION OF 6XXX ALLOY INGOTS WITH AN ADDITION OF VANADIUM*.
- [17] Lech-Grega, M., Szymanski, W., Plonka, B., Boczekal, S., Gawlik, M., & Korczak, P. (2013). *THE STRUCTURE AND PROPERTIES OF WROUGHT ALUMINIUM ALLOYS SERIES 6XXX WITH VANADIUM FOR AUTOMOTIVE INDUSTRY"*. www.imn.skawina.pl

- [18] Lodgaard, L., & Ryum, N. (2000). Precipitation of dispersoids containing Mn and/or Cr in Al-Mg-Si alloys. In *Materials Science and Engineering* (Vol. 283). www.elsevier.com/locate/msea
- [19] Martin, J. W. (1980). *Micromechanisms in Particle-Hardened Alloys*. Cambridge University Press.
- [20] Meng, Y., Cui, J., Zhao, Z., & Zuo, Y. (2013). Effect of vanadium on the microstructures and mechanical properties of an Al-Mg-Si-Cu-Cr-Ti alloy of 6XXX series. *Journal of Alloys and Compounds*, 573, 102–111. <https://doi.org/10.1016/j.jallcom.2013.03.239>
- [21] Miao, W. F., & Laughlin, D. E. (2000). *Effects of Cu Content and Preaging on Precipitation Characteristics in Aluminum Alloy 6022*.
- [22] Mondolfo, L.F. (1976) *Aluminum Alloys: Structure and Properties*. Butterworths and Co., Ltd., London, 806. <http://dx.doi.org/10.1016/B978-0-408-70932-3.50404-6>
- [23] Villars, P. (1997). *Pearson's Handbook Desk Edition*. ASM International, Materials Park, OH.
- [24] Wang, X., Poole, W. J., Esmaili, S., Lloyd, D. J., & Embury, J. D. (2003). *Precipitation Strengthening of the Aluminum Alloy AA6111* (Vol. 34).
- [25] Wyckoff, R.W.G. (1963). *Crystal Structures*. John Wiley, New York.